

Layered Atlantic Smoke Interactions with Clouds (LASIC) Field Campaign Report

P Zuidema	M Alvarado
C Chiu	S DeSzoeka
C Fairall	G Feingold
A Freedman	S Ghan
J Haywood	P Kollias
E Lewis	G McFarquhar
A McComiskey	D Mechem
T Onasch	J Redemann
D Roms	D Turner
H Wang	R Wood
S Yuter	P Zhu

May 2018



DISCLAIMER

This report was prepared as an account of work sponsored by the U.S. Government. Neither the United States nor any agency thereof, nor any of their employees, makes any warranty, express or implied, or assumes any legal liability or responsibility for the accuracy, completeness, or usefulness of any information, apparatus, product, or process disclosed, or represents that its use would not infringe privately owned rights. Reference herein to any specific commercial product, process, or service by trade name, trademark, manufacturer, or otherwise, does not necessarily constitute or imply its endorsement, recommendation, or favoring by the U.S. Government or any agency thereof. The views and opinions of authors expressed herein do not necessarily state or reflect those of the U.S. Government or any agency thereof.

Layered Atlantic Smoke Interactions with Clouds (LASIC) Field Campaign Report

P Zuidema, University of Miami
Principal Investigator

M Alvarado, Atmospheric and Environmental Research
C Chiu, Colorado State University
S DeSzoek, Oregon State University
C Fairall, University of Colorado (UC)
G Feingold, National Oceanic and Atmospheric Administration
A Freedman, Aerodyne Research, Inc. (ARI)
S Ghan, Pacific Northwest National Laboratory (PNNL)
J Haywood, University of Exeter
P Kollias, McGill University
E Lewis, Brookhaven National Laboratory
G McFarquhar, University of Oklahoma
A McComiskey, UC
D Mechem, University of Kansas
Tim Onasch, ARI
Jens Redemann, National Aeronautics and Space Administration
D Romps, Lawrence Berkeley Laboratory
D Turner, National Severe Storms Laboratory
H Wang, PNNL
R Wood, University of Washington
S Yuter, North Carolina State University
P Zhu, Florida International University
Co-Investigators

May 2018

Work supported by the U.S. Department of Energy,
Office of Science, Office of Biological and Environmental Research

Executive Summary

Southern Africa is the world's largest emitter of biomass burning aerosols. Their westward transport over the remote southeast Atlantic Ocean co-locates some of the largest atmospheric loadings of absorbing aerosol with the least examined of the Earth's major subtropical stratocumulus decks. Global aerosol model results highlight that the largest positive top-of-atmosphere (TOA) forcing in the world occurs in the southeast Atlantic, but this region exhibits large differences in magnitude and sign between reputable models, in part because of high variability in the underlying model cloud distributions. Many uncertainties contribute to the highly variable model radiation fields: the aging of the shortwave-absorbing aerosol during transport, how much of the aerosol mixes into the cloudy boundary layer, and how the low clouds adjust to smoke-radiation and smoke-cloud interactions. In addition, the ability of the biomass burning aerosol to absorb shortwave radiation is known to vary seasonally as the fuel type on land changes.

LASIC (Layered Atlantic Smoke Interactions with Clouds) is a strategy to improve our understanding of aged carbonaceous aerosol, its seasonal evolution, and the mechanisms by which clouds adjust to the presence of the aerosol. The observational strategy centers on deploying the U.S. Department of Energy (DOE) Atmospheric Radiation Measurement (ARM) Climate Research Facility first ARM Mobile Facility (AMF1) cloud, aerosol, and atmospheric profiling instrumentation to Ascension Island, located within the trade-wind shallow cumulus regime (14.50W, 80S) 3000 km offshore of continental Africa. The location is within the latitude zone of the maximum outflow of aerosol, with the deepening boundary layer known to entrain free-tropospheric smoke.

The primary activities for LASIC are: 1) to improve current knowledge on aged biomass burning aerosol and its radiative properties as a function of the seasonal cycle; 2) to use surface-based remote sensing to sensitively interrogate the atmosphere for the relative vertical location of aerosol and clouds; 3) to improve our understanding of the cloud adjustments to the presence of shortwave-absorbing aerosol within the vertical column, both through aerosol-radiation and through aerosol-cloud interactions; 4) to aid low cloud parameterization efforts for climate models. The measurements span June 1, 2016-October 31, 2017, encompassing two July-October biomass burning seasons. The August-September, 2016, months include an intensive operational period (IOP) with 8x/daily radiosondes. In 2017, from 16 August through 7 September, the United Kingdom Facility for Airborne Atmospheric Measurements (FAAM) BAe-146 plane was deployed from Ascension, providing complementary data on the atmosphere's vertical structure as part of the Cloud-Aerosol-Radiation Interactions and Forcing (CLARIFY) project, with similar scientific goals. The National Aeronautics and Space Administration (NASA) Observations of Clouds above Aerosols and their Interactions (ORACLES) aircraft campaign, sharing similar objectives to LASIC, deployed from Namibia in September, 2016, and Sao Tome in August, 2017. The latter included a suitcase flight to Ascension spanning August 18-21. In 2017 a cavity-attenuated phase shift single-scattering albedo (CAPS-SSA) instrument belonging to Aerodyne was brought to Ascension, gathering data primarily for August, towards providing a second, independent measurement of aerosol absorption. Ascension Island is also an Aerosol Robotic Network (AERONET) site.

Acronyms and Abbreviations

3D	three-dimensional
ABE	aerosol best estimate
ACSM	aerosol chemistry speciation monitor
AERI	atmospheric emitted radiance interferometer
AEROCLO	Aerosols, Radiation and Clouds in Southern Africa
AeroCom	Aerosol Comparisons between Observations and Models
AERONET	Aerosol Robotic Network
AETH	aethelometer
AGU	American Geophysical Union
Air MSPI	airborne multiangle spectro-polarimeter imager
AMF	ARM Mobile Facility
AMSR-E	Advanced Microwave Scanning Radiometer-Earth Observe System
ARM	Atmospheric Radiation Measurement
ASP	Aerosol Simulation Program
BB	biomass burning
CALIOP	Cloud Aerosol Lidar with Orthogonal Polarization
CAM5	Community Atmosphere Model (NCAR)
CAPS	cavity-attenuated phase shift
CAPT	Cloud-Associated Parameterizations Testbed
CERES	Clouds and Earth's Radiant System
CESM	Community Earth System Model
CHARTS	Code for High-resolution Accelerated Radiative Transfer with Scattering
CLARIFY	Cloud-Aerosol-Radiation Interactions and Forcing
CMIP	Coupled Model Intercomparison Project
CPC	condensation particle counter
DOE	U.S. Department of Energy
ECMWF	European Centre for Medium-Range Weather Forecasts
EECRA	Extended Edited Synoptic Cloud Reports Archive
eMAS	enhanced MODIS Airborne Simulator
ERA-Interim	ECMWF global atmospheric reanalysis from 1979
FAAM	Facility for Airborne Atmospheric Measurements
GLOMAP	Global Model of Aerosol Processes
GNDRAD	ground radiometers on stand for upwelling radiation
HTDMA	hygroscopic tandem differential mobility analyzer
HYSPLIT	Hybrid Single-Particle Lagrangian Integrated Trajectory (NOAA model)

IGRA	Integrated Global Radiosonde Archive
INDOEX	Indian Ocean Experiment
IOP	intensive operational period
IPCC	Intergovernmental Panel on Climate Change
ISCCP	International Satellite Cloud Climatology Project
KASACR	Ka-band scanning ARM cloud radar
LASIC	Layered Atlantic Smoke Interactions with Clouds
LBLRTM	Line-By-Line Radiative Transfer Model
LES	large-eddy simulation
LWP	liquid water path
MAOS	mobile aerosol observing system
MET	surface meteorological instrumentation
Met	Meteorological
MFR	multifilter radiometer
MFRSR	multifilter rotating shadowband radiometer
MMF	multi-scale modeling framework
MODIS	Moderate Resolution Imaging Spectroradiometer
MPL	micropulse lidar
MPLNET	Micro-Pulse Lidar Network (NASA)
MWR3C	3-channel microwave radiometer
NASA	National Aeronautics and Space Administration
NCAR	National Center for Atmospheric Research
NCCN	cloud condensation nuclei number
NFOV	Narrow field of view
NIR	near infrared
NOAA	National Oceanic and Atmospheric Administration
ORACLES	Observations of Clouds above Aerosols and their Interactions
ORG	optical rain gauge
PASS	photo-acoustic soot spectrometer
PCASP	passive cavity aerosol spectrometer
PNNL	Pacific Northwest National Laboratory
POP	precipitation of probability
PSAP	particle soot absorption photometer
PTRMS	proton transfer mass spectrometer
rBC	refractory black carbon
RH	relative humidity
RICO	Rain in Cumulus over the Ocean
RWP	radar wind profiler

SAFARI 2000	Southern African Regional Science Initiative
SASHE	shortwave array spectroradiometer-hemispheric
SASZE	shortwave array spectroradiometer-zenith
SEBS	surface energy balance system
SEVIRI	Spinning Enhanced Visible and Infrared Imager
SKYRAD	sky radiometers on stand for downwelling radiation
SMPS	scanning mobility particle sizer
SOA	secondary organic aerosol
SODAR	sonic detection and ranging
SONDE	balloon-borne sounding system
SP2	single-particle soot photometer
SS	supersaturation
SSA	single-scattering albedo
SSFR	solar spectral flux radiometer
SST	sea surface temperature
TSI	total sky imager
TWRCAM	tower camera
UHSAS	ultra-high-sensitivity aerosol spectrometer
UK	United Kingdom
UTC	Coordinated Universal Time
VAMOS	Variability of the American Monsoon System
VAP	value-added product
VBS	Volatility Basis Set
VCEIL	ceilometer
VIIRS	Visible Infrared Imaging Radiometer Suite
VOCALS	VAMOS Ocean-Cloud-Atmosphere-Land Study
WACR	W-band ARM cloud radar
WSACR	W-band scanning ARM cloud radar

Contents

Executive Summary	iii
Acronyms and Abbreviations	iv
1.0 Background.....	1
1.1 Introduction	1
1.2 Smoke Radiation and Composition.....	4
1.3 Smoke-Cloud Interactions.....	4
2.0 LASIC Activities, Goals, Hypotheses, and Instrument Tables.....	6
3.0 Specific Objectives	8
3.1 Characterizing Aged Carbonaceous Aerosol	8
3.2 Accurate Identification of Aerosol-Cloud Vertical Structure	10
3.3 Cloud Adjustments to Aerosol-Radiation and Aerosol-Cloud Interactions	11
3.4 Distinguishing Aerosol from Meteorological Effects	13
3.5 Measurements that Span the Full Annual Cycle and Low Cloud Model Parameterization Development Support.....	14
4.0 Site Description, Planning, Value-Added Products, and Collaborations	16
4.1 Site Description.....	16
4.2 Related Campaigns.....	18
4.2.1 CLARIFY and ORACLES.....	18
4.2.2 The LASIC SSA Constraint Study.....	19
4.2.3 Supplemental Measures for the LASIC Campaign	19
5.0 Highlights	19
6.0 Results	23
7.0 Public Outreach	25
8.0 LASIC Publications.....	25
8.1 Journal Articles/Manuscripts.....	25
8.2 Meeting Abstracts/Presentations/Posters	25
9.0 References	26

Figures

1	Left-hand panel: The September mean SST and cloud fraction highlights the large southeast Atlantic stratocumulus region. Right-hand panel: Clouds and Earth’s Radiant System (CERES) annual-mean net cloud radiative forcing for March 2000-February 2001.....	1
2	Estimates of the August-September top-of-atmosphere direct radiative forcing from 12 global aerosol models with prescribed radiative properties	2
3	During September, 600 hPa winds escort the BB aerosol from fires in continental Africa westward over the entire south Atlantic stratocumulus deck.	3
4	From left to right: vertical profiles of passive cavity aerosol spectrometer (PCASP)	3
5	a) Precipitation susceptibility as a function of LWP in AMF data and from VAMOS Ocean-Cloud-Atmosphere-Land Study (VOCALS) and Rain in Cumulus Over the Ocean (RICO) large-eddy simulation (LES) data sets.....	6
6	CALIOP snapshots of 532-micron backscattered intensity near Ascension Island suggests a range of cloud-aerosol interactions.	10
7	a)-g) Monthly-mean profiles of atmospheric potential temperature, relative humidity, and mixing ratio clearly highlight the warmer, deeper, and moister boundary layer at Ascension Island compared to St. Helena, and the distinct seasonal cycle at each location.....	14
8	The annual cycle in left) cloud amount and right) liquid water path over the 100-200°S, 0-100°E region in Coupled Model Intercomparison Project (CMIP)5 models and observations.....	15
9	Leftmost panel: Ascension Island seen in profile. The rightmost panel indicates the location of Ascension within the southeast Atlantic using MODIS satellite imagery.....	17
10	Ascension Island layout of instrumentation.	17
11	14 August 1200 UTC-16 August 00 UTC time series of the micropulse-lidar	20
12	27-member ensemble HYSPLIT back trajectories initialized on 13 August 2016 12 UTC originating from Ascension Island	22
13	Cavity-attenuated phase shift (CAPS) and particle soot absorption photometer (PSAP) aerosol light absorption measurements for late August, 2016, Ascension Island.....	23
14	1 June-31 October, 2016 time series of a) single-particle soot photometer (SP2)-derived refractory black carbon (rBC) mass concentrations.	24

Tables

1	AMF1 instruments.....	7
---	-----------------------	---

1.0 Background

Note: This description is an updated version of what was stated in the LASIC Science Plan.

1.1 Introduction

The southeast Atlantic net cloud radiative forcing attains a global maximum on par with that of the southeast Pacific (Lin et al. 2010; Figure 1). Southerly near-surface winds stream equatorward after their anticyclonic rotation around the south Atlantic sea level pressure high. Lower free-tropospheric winds (~ 700 hPa), in contrast, are primarily driven by a deeper anticyclone based over southern Africa. These warm winds combine with the cool sea surface temperatures to encourage the formation of a large stratocumulus deck, transitioning to year-round trade-wind shallow cumulus at the location of Ascension Island (14.5°W , 8°S ; Figure 1). This remote but populated volcanic island was the location selected for the first ARM Mobile Facility (AMF1) deployment from June 1, 2016 to May 31, 2017.

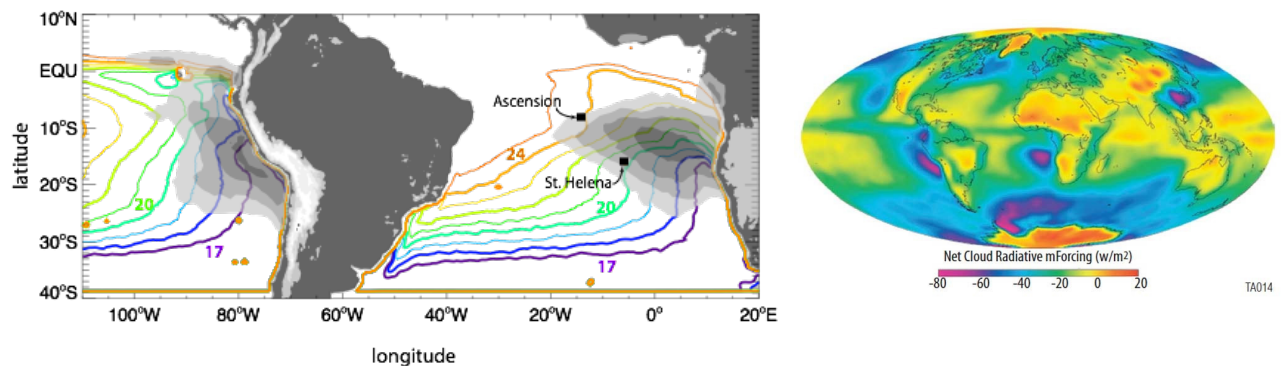


Figure 1. Left-hand panel: The September mean SST and cloud fraction highlights the large southeast Atlantic stratocumulus region. SST from 1998-2013 Thematic Microwave Imager (labeled colored contour lines in degrees Celsius) and low cloud fraction from 2000-2012 Moderate Resolution Imaging Spectroradiometer (MODIS; grey shading spans 0.6-1). Land topography in 1-km height increments. Right-hand panel: Clouds and Earth's Radiant System (CERES) annual-mean net cloud radiative forcing for March 2000-February 2001, from <http://npp.gsfc.nasa.gov>.

An unexamined low-cloud regime for the U.S. Department of Energy (DOE) Atmospheric Radiation Measurement (ARM) Climate Research Facility is interactions of shallow clouds with biomass-burning aerosols. Such aerosols absorb as well as scatter shortwave radiation, and shortwave-absorbing aerosols are capable of providing a positive impact on climate (a warming), in contrast to the cooling provided by aerosols, such as sulfate particles, that only scatter shortwave radiation. The separate contribution of biomass burning aerosols to the global climate is highlighted within the Technical Summary of the most recent 2014 Intergovernmental Panel on Climate Change (IPCC) report, where the global radiative forcing is estimated at $+0.2-0.5 \text{ W m}^{-2}$ (Boucher et al. 2013). The contribution to regional climate, particularly over the southeast Atlantic, is much larger.

Global aerosol model estimates of the direct radiative effect of the aerosols alone, even when the aerosol radiative properties are identically prescribed, vary widely, as shown in Figure 2. The Aerosol Comparisons between Observations and Models (AeroCom) project, an open call to aerosol modeling groups to compare their models using identical set-ups, has focused on providing comprehensive assessments of the aerosol life cycle in participating models (Kinne et al. 2006; Schultz et al. 2006; Textor et al. 2006; Stier et al. 2013; Myrhe et al. 2013). The AeroCom top-of-atmosphere results demonstrate that, in the mean, the largest positive TOA forcing in the world occurs in the southeast Atlantic, but, that this region also exhibits large differences in magnitude and sign between reputable models. This is also consistent with high variability in the underlying model cloud distributions (Stier et al., 2013), and differences in the aerosol vertical distribution (Koffi et al. 2012). The AeroCom project is planning a future activity with a focus on biomass burning aerosol effects. de Graaf (2012) used high-spectral-resolution satellite data to show that the instantaneous direct radiative effect of biomass burning (BB) aerosol over clouds in the SE Atlantic region can exceed $+130 \text{ W m}^{-2}$ instantaneously, and $+23 \text{ W m}^{-2}$ in the monthly mean (de Graaf et al. 2014). These values are far higher than those diagnosed in climate models, whose monthly-mean regional values reach only $+5 \text{ W m}^{-2}$ (Figure 2). This suggests a possible universal model underestimate.

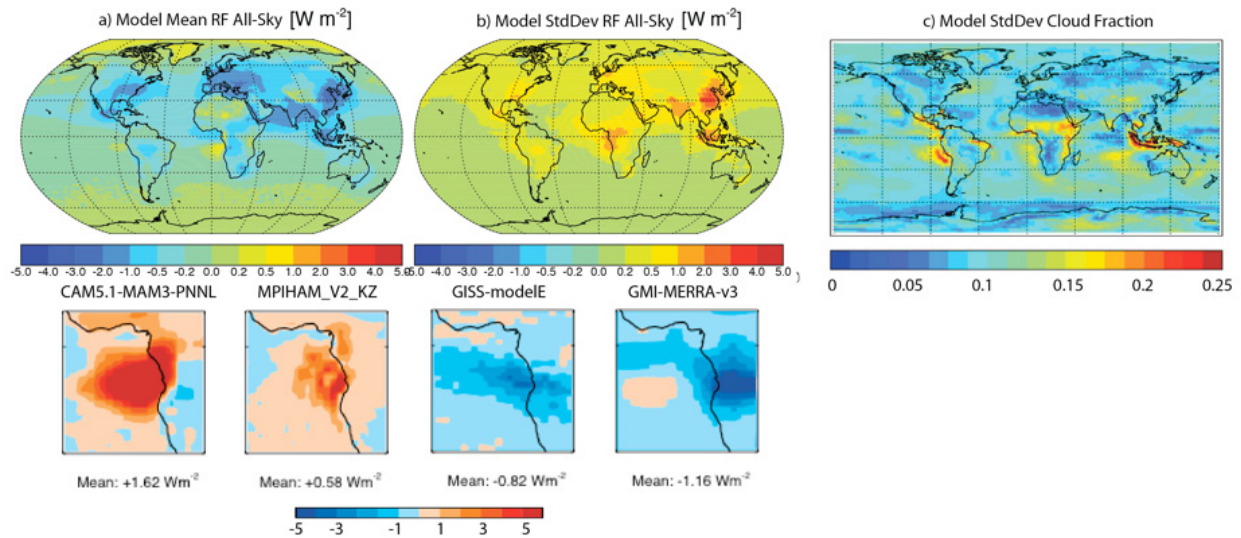


Figure 2. Estimates of the August-September top-of-atmosphere direct radiative forcing from 12 global aerosol models with prescribed radiative properties (Stier et al. 2013) highlight that a) the largest positive forcing is in the southeast Atlantic, but b) model results vary significantly, c) in part because of differences in cloud fraction.

Ascension Island is subject to the free-tropospheric BB emissions emanating from Africa (Figure 3). The largest consumption of biomass by fire in the world occurs in Africa (van der Werf et al. 2006; 2010; Granier et al. 2011), with the global majority of aerosols overlying clouds occurring in the southeast Atlantic (Waquet et al. 2013). The BB aerosol extends well into the trade-wind cumulus region, where the deepening boundary layer and subsiding aerosol layer are more likely to directly interact (Figure 3, inset). Few observations from the remote southeast Atlantic are available, however, with satellite measurements not yet able to determine the extent to which aerosol is entrained into the boundary layer. Vertical profile data from one United Kingdom (UK) Meteorological (Met) Office research flight to Ascension Island as part of the Southern African Regional Science Initiative (SAFARI 2000) show enhanced aerosol

concentrations within the boundary layer (Figure 4). Longer-term aerosol statistics, such as will be available from the DOE AMF1 platform, will provide a definitive climatology both at the surface and of the vertical structure, placing such anecdotal evidence on stronger footing.

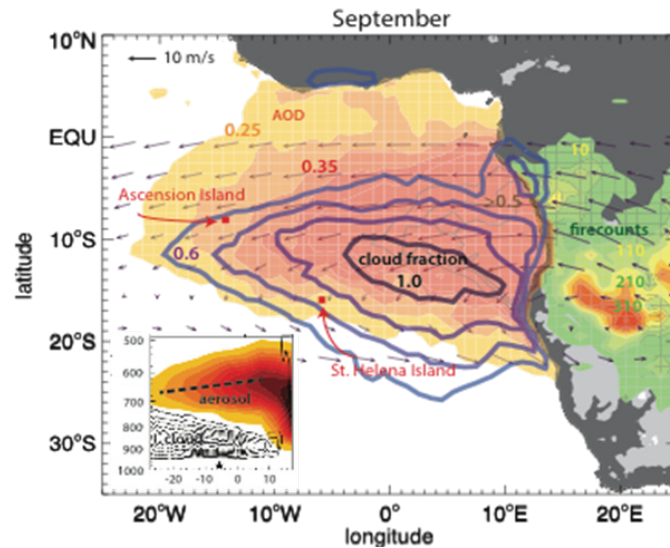


Figure 3. During September, 600 hPa winds escort the BB aerosol (optical depth in warm colors) from fires in continental Africa (green to red, firecounts) westward over the entire south Atlantic stratocumulus deck (cloud fraction in blue contours). The inset, a 6°S-17°S longitude slice, highlights the main aerosol outflow occurring at 10°S, subsiding to the north where the boundary layer also deepens. Main figure is based on MODIS 2002-2012 data and the ERA-Interim Reanalysis, inset on the space-based Cloud Aerosol Lidar with Orthogonal Polarization (CALIOP) and CloudSat 2006-2010 data. Reproduced from Zuidema et al. 2016.

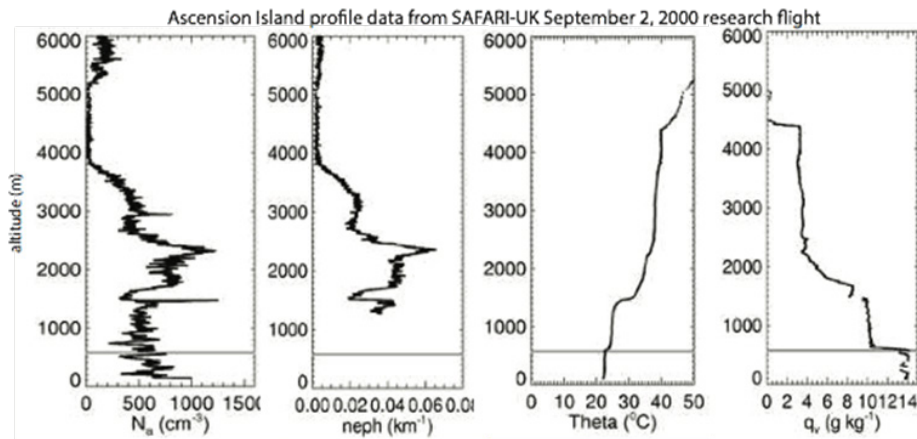


Figure 4. From left to right: vertical profiles of passive cavity aerosol spectrometer (PCASP) accumulation-mode aerosol concentration and the nephelometer scattering coefficient at 0.55 micron indicate aerosol concentrations exceeding 500 cm^{-3} in the boundary layer, with the potential temperature and water vapor mixing ratio profiles indicating two well-mixed layers. The grey line indicates cloud base height. Data sampled while descending near Ascension Island on September 2, 2000, courtesy of Steve Abel, UK Met Office.

1.2 Smoke Radiation and Composition

At the top of the atmosphere, the direct radiative effect of the biomass burning aerosol is positive (a warming) when the aerosol is located above a bright cloud deck, and negative (a cooling) when above a dark ocean surface (e.g., Remer 2009). For a typical BB aerosol single-scattering albedo (SSA) of 0.9, the cloud fraction above which the aerosol exerts an overall warming has been estimated as approximately 0.4 (Russell et al. 1997; Abel et al. 2005; Chand et al. 2009; Seidel and Popp 2012), based on plane-parallel radiative transfer calculations constrained by satellite data. The cumulus clouds most prevalent at Ascension are not well modeled radiatively by the plane-parallel assumption, however (e.g., Zuidema et al. 2008). It is also worth stressing that small changes in aerosol SSA have a disproportionate impact on the sign of the net top-of-atmosphere radiative forcing (Haywood and Shine 1995). How the absorbing aerosol ages during transport, thereby affecting the SSA, is not well known, with current surface-based remote-sensing characterization limited to the AERONET site at Ascension Island (Satheesh et al. 2009). The comparison of the SSA deduced from the in situ profile shown in Figure 4 to those over mainland Africa would estimate that the single-scattering albedo increases from 0.84 over mainland Africa, to 0.91 during the week-long transit to Ascension (Haywood et al. 2003).

Most of the black carbon emanating from Africa is released by the open burning of grasslands, with incomplete combustion the norm (Bond et al. 2013). The emissions are thought to be accompanied by large organic aerosol components that also contribute to shortwave and ultraviolet absorption, with the fractional attribution uncertain. The mass absorption cross-section for black carbon can thereby increase by approximately 50% as the black carbon becomes internally mixed with other aerosols. AERONET SSA measurements over land also show a seasonal evolution of SSA from 0.85 to near 0.9 (Eck et al. 2013), attributed to changes in fuel types as the biomass burning shifts further to the south. The change of the net radiative properties of the biomass burning aerosol from July to November is therefore also poorly known. The unprecedented sampling throughout the full annual cycle afforded by LASIC will answer the question of whether and how the radiative properties of the smoke evolve offshore as well as over land.

1.3 Smoke-Cloud Interactions

As the BB aerosol flows out over the Atlantic Ocean, remarkable and poorly understood interactions with low clouds occur. These depend crucially on the relative vertical location of the BB aerosol to the cloud deck. When the smoke is situated directly above the cloud field, the stabilization of the atmosphere through warming further supports the cloud field, thickening the cloud and increasing the cloud fraction (Johnson et al. 2004). Such a cloud adjustment appears to find observational support in satellite analyses (Loeb and Schuster 2008; Wilcox 2010, 2012; Adebisi et al. 2014). The enhanced cloudiness constitutes a potentially substantial contribution to the net effective radiative forcing that exceeds that from the aerosol alone, capable of increasing the surface cooling from $\sim 0.2\text{K}$ to 2K (Sakaeda et al. 2011). An almost unexplored process issue, however, is the mechanism by which atmospheric warming and aerosol scattering that is maximized at the level of maximum aerosol density at $\sim 650\text{ hPa}$, is transmitted to the boundary layer cloud residing $\sim 200\text{ hPa}$ below. The impact of shortwave attenuation by aerosol scattering upon the cloudy boundary layer, for example by discouraging decoupling within the boundary layer, as well as the longwave impact of the anomalous moisture present within the aerosol layer (Adebisi et al. 2015), should also be considered.

If the BB aerosol is located within the cloudy boundary layer, the shortwave absorption warms the cloud and surrounding atmosphere, lowering the relative humidity and thereby the cloudiness (Ackerman et al. 2000; Johnson et al. 2004; McFarquhar and Wang 2006; Hill and Dobbie 2008; Koch and Del Genio 2010). BB aerosols can also become entrained into the clouds themselves. While black carbon is hydrophobic, other aerosols, particularly organic aerosols, coalesce with the black carbon during transport and increase its hygroscopicity and thereby effectiveness as a cloud condensation nuclei. Cloud processes such as nucleation and impact scavenging in turn affect the aerosol mass, and feed back further into the ability of the aerosol to act as a cloud condensation nuclei. Results from the SAFARI campaign indeed suggest that CCN increase in aged BB plumes (Ross et al. 2003). The activated aerosol can then provide a radiative forcing through their reduction of the mean drop size, all else held constant (Twomey 1977). There is large-scale evidence of altered microphysics from BB aerosol in the southeast Atlantic from satellite analyses (Constantino and Breon 2010, 2013, Painemal et al. 2015).

The activated aerosol can also affect the likelihood of precipitation (e.g., Feingold and Seibert 2009; Wang et al. 2010; Terai et al. 2012). From DOE measurements collected in the Azores, the rainrate at cloudless R_{cb} is proportional to liquid water path (LWP) as $LWP^{1.68 \pm 0.05}$ with an assumed supersaturation of 0.55% (Mann et al. 2014). How these exponents change when absorbing smoke particles become the dominant aerosol type, and whether models reproduce these power relationships well are of great interest. Additionally, the precipitation susceptibility to the cloud condensation nuclei number (NCCN) ranges between 0.5 and 0.9 and generally decreases with LWP (as shown in Figure 5a). Precipitation susceptibility estimates are not yet known reliably for clouds impacted by long-range BB aerosol transport. Measurements from LASIC will provide an excellent opportunity to enhance analysis and intercomparisons of precipitation susceptibility to other aerosol proxies (such as aerosol optical depth, and aerosol index), and to help resolve outstanding discrepancies among various studies.

The susceptibility of precipitation of probability (POP) to N_{CCN} (S_{POP}) also varies between observations from ground-based and aircraft deployments (Figure 5b) and satellites and simulations (Figure 5c). S_{POP} from AMF data is higher than that derived from CloudSat, and equivalent with that from aircraft observations (Figure 5b) and high-resolution simulations (Figure 5c). This indicates that the high-resolution multi-scale climate model may have already had the ability to represent aerosol-cloud-precipitation interactions properly. More experiments such as intercomparison between high-resolution ground-based measurements and simulations over other sites for a longer time period will provide further valuable confirmation. Ultimately this focus can be used to improve global models; these currently significantly overestimate drizzle frequency, calling into question the fidelity with which the second indirect effect of aerosol is captured.

For BB aerosol, the indirect effects must be compared in relative magnitude against at times opposing semi-direct effects, if, e.g., clouds are brightened as their cloud drop sizes decrease, but overall cloud fractions decrease (e.g., McFarquhar et al. 2004b; Johnson 2005). The recent availability of scanning cloud radars within the DOE mobile deployment pool raises the intriguing possibility that ‘cloud burn-off’ and changes in microphysics can be simultaneously observed as a function of the boundary-layer absorbing aerosol concentration.

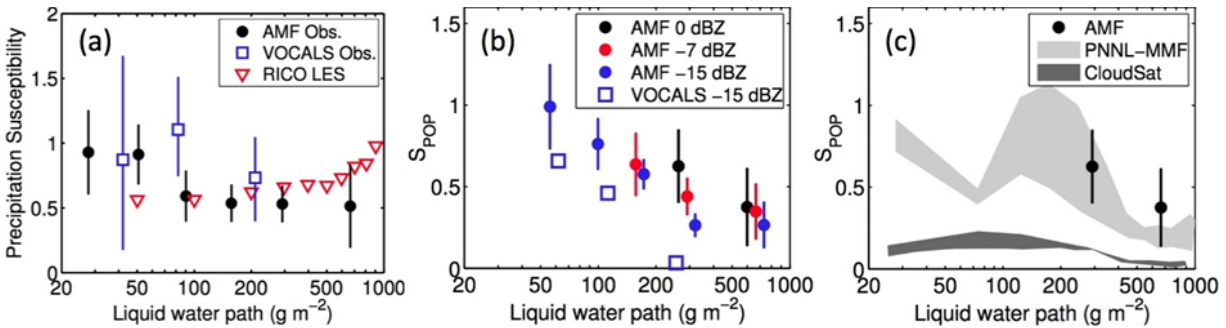


Figure 5. a) Precipitation susceptibility as a function of LWP in AMF data (with respect to N_{CCN}) and from VAMOS Ocean-Cloud-Atmosphere-Land Study (VOCALS) and Rain in Cumulus Over the Ocean (RICO) large-eddy simulation (LES) data sets (with respect to N_d ; Terai et al. 2012; Sorooshian et al. 2009). Susceptibility of POP (S_{POP}) from b) AMF data and VOCALS, and c) CloudSat data and Pacific Northwest National Laboratory (PNNL)-multi-scale modeling framework (MMF) outputs at 4-km resolution (Wang et al. 2012).

2.0 LASIC Activities, Goals, Hypotheses, and Instrument Tables

LASIC proposed four activities:

1. Improve current knowledge on the aging during transport of biomass burning aerosol radiative properties as a function of the seasonal cycle.
2. Establish the aerosol-cloud vertical structure.
3. Improve our understanding of the cloud adjustments to the presence of shortwave-absorbing aerosol within the vertical column, both through aerosol-radiation and aerosol-cloud interactions.
4. Provide observations aiding low cloud parameterization efforts for climate models.

Aerosol-free conditions within the measurements of the full annual cycle provide a reference state, and the mean evolution of smoke properties will be evaluated between July and November. The LASIC campaign consists of a deployment of AMF1 instrumentation (the Mobile Aerosol Observing System [MAOS] and ground-based remote sensors) from June 1, 2016 through October 31, 2017 (see Table 1 for a complete list of instrumentation). An intensive operational period (IOP) consisting of 8x/daily radiosondes for two months is designated to coincide with the UK and National Aeronautics and Space Administration (NASA) aircraft deployments (detailed further below) and with the highest aerosol loading, from August 1-September 31, 2016. This characterization of the diurnal cycle of the boundary-layer thermodynamic and kinematic vertical structure is unprecedented for the southeast Atlantic. This characterization will be maintained at 4x/daily radiosondes during the rest of the deployment.

LASIC scientific goals are articulated through the following hypotheses:

Hypothesis 1 (H1): The single-scattering albedo of the carbonaceous aerosol overlying Ascension increases during the BB season as has been documented over land.

Hypothesis 2 (H2): Low-cloud properties at Ascension vary as a function of the amount, vertical distribution, and optical properties of absorbing aerosol aloft that is distinct from meteorology.

Hypothesis 3 (H3): Carbonaceous aerosol are present within the Ascension Island boundary layer, where they are capable of affecting cloud microphysics, precipitation susceptibility, and the cloud mesoscale organization.

Hypothesis 4 (H4): The evolution of the cloudy boundary layer between St. Helena and Ascension Island varies as a function of the absorbing aerosol loadings aloft as well as large-scale environmental parameters such as sea surface temperature.

LASIC science goals and objectives will be achieved by:

1. Characterizing the microphysical and optical properties of the carbonaceous aerosol at Ascension Island as a function of time.
2. Characterizing the low-cloud properties at Ascension Island as a function of the vertical location and optical properties of the absorbing aerosol within the atmospheric column, controlled for thermodynamic state and prior cloud evolution.
3. When carbonaceous aerosol is present within the boundary layer, assessing the aerosol size distribution and hygroscopicity, and relating the aerosol properties to the cloud spatial distribution, its microphysics, precipitation susceptibility, and cloud mesoscale organization.
4. Assessing the evolution of the cloudy boundary layer from St. Helena to Ascension Island under a wide range of atmospheric aerosol conditions as well as large-scale environmental conditions.

Table 1 lists the specific AMF1 instrumentation requests for Ascension. These include the MAOS-Aerosol and MAOS-Chemistry (MAOS-A and MAOS-C) packages, which we anticipate will be relocated directly from the GoAmazon deployment in Brazil to Ascension Island. Priority instruments are identified through an asterisk. Further planning details, including additional anticipated and desired instrumentation, and campaign-specific priorities including value-added products (VAPs) are contained in Section 4.

Table 1. AMF1 instruments.

MAOS baseline instrument	Function
Sonic Detection and Ranging (SODAR) System	Wind velocity in the lower atmosphere
Ultra-High-Sensitivity Aerosol Spectrometer (UHSAS)*	Aerosol size and number, 50 nm-1 micron
Dual-column CCN counter*	Number of activated aerosols at 2 supersaturations
Single-particle soot photometer (SP2)*	Black carbon mass and size
Scanning mobility particle sizer (SMPS)*	Aerosol size distribution, 15-450 nm
Photo-acoustic soot photometer (PSAP)*	Aerosol absorption and scattering coefficient at 3 wavelengths
Humidigraph (scanning RH w/ 3 single-wavelength nephelometers)*	Aerosol scattering coefficient as a function of relative humidity
Nephelometer, 3 wavelength*	Aerosol scattering coefficient
Condensation particle counter (CPC)*	Condensation particle concentration, 10 nm->3000 nm particle size
Condensation particle counter (CPC2)*	Condensation particle concentration, 2.5 nm->3000 nm particle size

MAOS baseline instrument	Function
Hygroscopic tandem differential mobility analyzer (HTDMA)*	Aerosol growth factor as function of humidity
Particle soot absorption photometer (PSAP)*	Aerosol extinction/absorption (black carbon)
7-wavelength aethelometer (AETH)*	Aerosol extinction/absorption (black carbon)
Weather transmitter (WXT-520)*	T, RH, u, v, rainfall, p
Aerosol chemistry speciation monitor (ACSM)*	Aerosol mass and composition
Radar wind profiler (RWP) (if available)	Wind vertical structure
MAOS-Chemistry (MAOS-C)	
Trace gas instrument system*	CO, SO ₂ , NO/NO ₂ /NO _y , O ₃
Proton transfer mass spectrometer (PTRMS)*	Volatile organic compounds
AMF1	
3-channel microwave radiometer (MWR3C)*	Integrated liquid water and water vapor
Balloon-borne sounding system (SONDE)* 4x/daily increasing to 8x/daily for 2 months	Temperature, humidity and wind vertical structure
Ceilometer (VCEIL)*	Cloud base
Radar wind profiler (RWP)*	Wind vertical structure
W-band scanning ARM cloud radar (WSACR)*	Cloud and precipitation spatial structure
W-band ARM cloud radar (WACR)*	Cloud and precipitation vertical structure
K-band scanning ARM cloud radar (KASACR)*	Cloud and precipitation spatial structure
Micropulse lidar (MPL)*	Aerosol vertical structure
Atmospheric emitted radiance interferometer (AERI)*	Cloud liquid water path and effective radii
Multifilter rotating shadowband radiometer (MFRSR)*	Aerosol optical depth
Narrow field of view (NFOV)*	Cloud optical depth and effective radius
Solar array spectrometer (SASHE and SASZE)*	Radiative closure
Surface energy balance system (SEBS)*	Surface energy balance. Soil moisture and flux measurements are not needed.
Surface radiation measurements (SKYRAD, MFR, GNDRAD)*	Surface radiation balance (overlap with SEBS?)
Surface meteorological instrumentation (MET)*	Surface-air-layer properties
Optical rain gauge (ORG)*	Surface rain
Tower camera (TWRCAM)*	Photo imagery
Total sky imager (TSI)*	Cloud fraction

3.0 Specific Objectives

3.1 Characterizing Aged Carbonaceous Aerosol (H1)

Most biomass burning aerosol measurements are taken close to their source. Yet, the carbonaceous aerosol that alter the radiative fluxes and heating rates over the Atlantic Ocean are already aged by at least a day, with the transport time to Ascension taking 5-6 days (Adebiyi and Zuidema 2016). In situ

characterization during SAFARI 2000 concluded that most of the aerosol aging occurs within the first few hours after leaving the source region (Abel et al. 2003), with the SSA rising by 5% over that time. Vakkari et al. (2014) similarly found that atmospheric oxidation and subsequent secondary aerosol formation drive large changes in BBA properties in the first 2-4 hours of transport. However, a satellite-based study suggests BB aerosol sizes and thereby the SSA continue to evolve during aerosol transport over the Atlantic (Waquet et al. 2013). Ascension is 3000 km from the African coast, and as such the comprehensive surface-based aerosol measurements possible with the Mobile Aerosol Observing System will assess the properties of the truly aged aerosol. Because the characterization is occurring so far from the biomass burning source, these surface-based aerosol characterizations can be considered representative of the carbonaceous aerosol properties throughout the vertical column. These surface-based measurements will characterize those properties of BB aerosols most needed to model the direct radiative forcing: the mass absorption and scattering cross-sections and mass concentrations. Measurements specifically aimed at characterizing the aerosol SSA include the photo-acoustic soot spectrometer (PASS), the Particle Soot Absorption Photometer (PSAP), the seven-wavelength aethelometer, and the humidigraph. The latter can assess the aerosol scattering coefficient using three different wavelength nephelometers as a function of relative humidity.

Closure studies will link absorption to measurements of BC mass and mixing state, such as from the single-particle soot photometer (SP2) and aerosol chemistry speciation monitor (ACSM). Column radiative closure studies with the MFRSR and shortwave array spectroradiometer-zenith (SASZE) on cloud-free days, alone or in combination with aerosol vertical profile information from the MPL (see Section 3.3), will characterize the column-average aerosol properties needed to match the observed surface radiance and thus provide information on the aerosol aloft. This work goes hand-in-hand with developing retrievals for the SASZE and shortwave array spectroradiometer-hemispheric (SASHE) spectral radiometers. The LASIC observations will provide an independent opportunity to evaluate the ARM 3-wavelength Aerosol Best Estimate (ABE). This will be done by comparing calculations from the Line-By-Line Radiative Transfer Model (LBLRTM)/Code for High-resolution Accelerated Radiative Transfer with Scattering (CHARTS) radiative transfer model (Mlawer et al. 2000) using the ABE profiles as inputs, to the observations of the SASZE and SASHE spectral radiometers near the ABE reference wavelengths. The SASZE and SASHE measurements will also lend themselves to better estimates of AOD, SSA, and g . Since these properties are largely determined by the aerosol composition and size distribution, the strategy is to determine the column-integrated aerosol size distribution and complex index of refraction (which is a function of aerosol composition) that is most consistent with the available SASZE and SASHE data, similar to the method of Kassianov et al. (2007) for the ARM MFRSR. Further co-located measurements of aerosol chemical composition, size distribution, and optical properties, along with knowledge of sources and air transport, will be evaluated in relation to column and profile properties from ground-based passive and active remote sensors, providing a fuller, more accurate characterization of the aerosol throughout the column.

Further measurements will assess the ability of the aerosol to act as a cloud condensation nuclei, with an ultra-high-sensitivity aerosol spectrometer (UHSAS) as well as a Scanning Mobility Particle Sizer (SMPS) providing the sizing over the dominant CN size ranges (50-1000 nm and 15 nm-450 nm, respectively). Such data sets will be combined with a dual-column cloud condensation nuclei counter capable of counting the number of aerosols activated into CCN at two representative and independently selected supersaturations. Such measurements are integral to providing constraints for aerosol-cloud modeling, including for the AeroCom project. In addition, efforts will be made to analyze the chemistry

of the carbonaceous aerosol. This will be done using the updated Aerosol Simulation Program (ASP), with updated gas-phase chemistry and the Volatility Basis Set (VBS) scheme for secondary organic aerosol (SOA) formation (Alvarado and Prinn 2009; Alvarado et al. 2014). This improved ASP version has been used to analyze the chemistry of a South Africa savannah fire smoke plume (Hobbs et al. 2003) and the Williams fire smoke plume in California sampled by Akagi et al. (2012).

3.2 Accurate Identification of Aerosol-Cloud Vertical Structure (Supports H2, H3, and H4)

As a first-order issue, the vertical distribution of the absorbing aerosol and low cloud and their spatial and temporal variability must be known before the radiative forcings and cloud adjustments can be adequately characterized. The importance of an accurate characterization, and our current lack of one, is worth emphasizing. Space-based lidar is currently our best source of information (e.g., Figure 6). From space, the optically thin aerosol layer base must be detected after the lidar signal is attenuated by the intervening aerosol. During the day, the vertical sampling is hampered by solar interference, so that retrieved daytime smoke base altitudes are placed 500 m higher in the mean compared to nighttime altitudes (Meyer et al. 2013). Thus, CALIOP cloud-aerosol separation statistics tend to suggest little cloud-aerosol overlap and therefore little aerosol entrainment into the cloudy boundary layer (Meyer et al. 2013), but this is contradicted by satellite studies of the clouds themselves (e.g., Constantino and Breon 2013; Painemal et al. 2014), and anecdotally by the available in situ data such as shown in Figure 4.

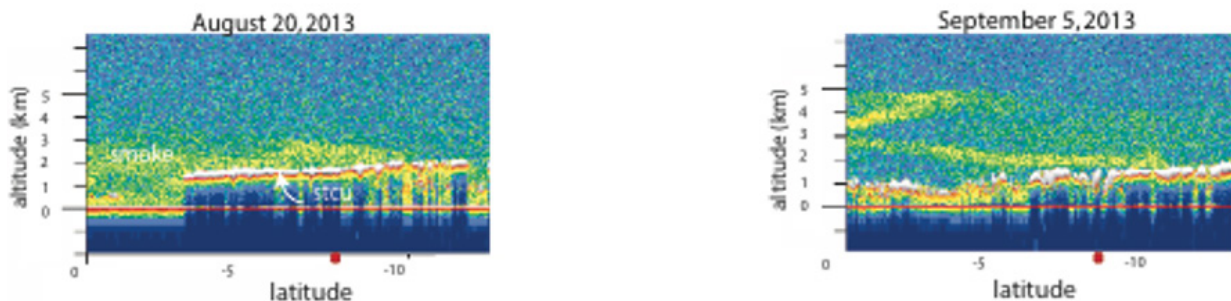


Figure 6. CALIOP snapshots of 532-micron backscattered intensity near Ascension Island suggests a range of cloud-aerosol interactions. Ascension’s latitudinal location is indicated as a red box on x-axis.

A definitive climatology of how often free-tropospheric aerosol interact with clouds rooted within the boundary layer requires long-term, high-time-resolution, surface-based lidars and radars. These provide much more detailed and vertically resolved profiles of aerosol and clouds than is possible from space. The aerosol vertical structure statistics also further our understanding of the transport and eventual deposition patterns of BB aerosol. The AMF1 micropulse cloud lidar (MPL) will be able to resolve the vertical structure to 30 m. Ascension Island is already an AERONET site, and the DOE MPL data set can potentially contribute constructively to a merged data set with the AERONET data. This will require coordination with NASA Micro-Pule Lidar Network (MPLNET) protocols (Welton et al. 2001). The surface-based W-band ARM cloud radar (WACR) primarily, and the scanning Ka-band and W-band ARM cloud radars (KASACR and WSACR), provide an accurate view of the cloud and precipitation vertical structure, resolved to 50 m, that will then be integrated with the lidar-derived aerosol statistics.

3.3 Cloud Adjustments to Aerosol-Radiation and Aerosol-Cloud Interactions (H2, H3)

If the surface-based aerosol measurements and vertically profiling lidar indicate that BB aerosol is present within the cloudy boundary layer, the ARM measurements will support scientific inquiry into the resulting cloud adjustments. These include what has colloquially been referred to as the “cloud burn-off” effect, whereby shortwave absorption by the aerosol raises the local temperature, reducing the relative humidity, and discouraging cloud growth. If this effect is also induced by BB aerosols entrained into boundary-layer cloud drops, a reduction in the mean drop size can occur for the same liquid water content, potentially reducing precipitation or enhancing evaporation even further. To date, the impact of entrained BB aerosol in the boundary layer has been examined for Indian Ocean Experiment (INDOEX) data (Ackerman et al. 2000) and the Amazon (e.g., Feingold et al. 2005). In both field experiments, the smoke was already present within the boundary layer.

The hyper spectral irradiance and radiance measurements from the scanning spectral Solar Array Spectrometer-Hemispheric and -Zenith (SASHE and SASZE) radiometers in the visible and near-infrared (NIR) regions will be applied to help separate the respective aerosol-cloud signatures. The NIR wavelengths reveal much more cloud fine structure than the visible wavelengths, mainly because the higher NIR-absorption by liquid water reduces the radiative smoothing effect of cloud multiple scattering. The better knowledge of cloud properties from the NIR wavelengths can then improve the characterization of aerosol optical properties towards achieving radiation closure.

Such measurements, when combined with the dual-wavelength scanning Ka-band and W-band ARM cloud radars (KASACR and WSACR) and with longer-term instruments possessing well-characterized retrieval algorithms, such as the Multifilter Rotating Shadowband Radiometer (MFRSR), Microwave Radiometer Profiler (MWRP), and a 3-channel and high-frequency Microwave Radiometer (MWR3C and MWRHF), are well-poised to provide insight into the relative magnitude of competing radiative effects from aerosols and clouds. The net radiative impact will be succinctly summarized by the downwelling radiation (SKYRAD) and surface energy balance system (SEBS) measurements, and surface-based rain gauges will assess how much precipitation reaches the surface and leaves the atmosphere. Precipitation susceptibility estimates can then be generated using the WACR-derived precipitation estimates, microwave-derived liquid water path, and the CCN-counter concentration values and other aerosol proxies.

As noted previously, such susceptibility metrics have been found to differ systematically from those derived using space-based remote sensing at larger scales (Figure 5), with implication for how these metrics are used to parameterize climate models. The long-term statistics from Ascension Island, occurring within a different aerosol-cloud regime, will provide an opportunity to test the universality of these results. These observational efforts will be coordinated with high-resolution modeling of aerosol-cloud processes.

The precipitation particle size distributions from the Joss-Waldvogel disdrometer and the optical rain gauge rainfall rate measurements will furthermore be used to adjust (calibrate) the radar wind profiler (RWP) power measurements using the techniques developed by Tridon et al. (2013). Using the newly proposed RWP operational modes, we will have cloud and precipitation observations from the surface throughout the full depth of the atmosphere with no attenuation. Combining the RWP with the WACR observations will provide a dual-wavelength view of clouds and precipitation. The RWP will also

contiguously map the inversion height (compared to the 4-8 daily measurements from the soundings) and help identify the entrainment episodes of free-tropospheric air that are so critical for bringing smoky free-tropospheric air into the boundary layer.

The Ka/W-band scanning ARM cloud radars (Kollias et al. 2014a) will provide information on the mesoscale structure and organization of the cloud fields (Kollias et al. 2014b), including on the horizontal wind fields in the cloud layer. The Ka/W-SACR will be used to track cloud structures and study the lifetime of isolated cumuli clouds (Borque et al. 2014). The recorded radar Doppler spectra can be used to assess the early drizzle growth (Kollias et al. 2011a, 2011b) as a function of variable aerosol conditions. From the constructed 3D cloud structure (Lamer et al. 2014), the 3D vertical velocity field can be retrieved and applied to entrainment studies using the profiling and scanning cloud radar observations.

When the absorbing aerosol layer is entirely located above the cloud, the stabilization of the atmosphere at that level may encourage cloudiness by discouraging the entrainment of warmer, drier air into the boundary layer. The absorbing aerosol layer aloft is typically associated with anomalous moisture (Adebiyi et al. 2015), aiding hygroscopic growth of the aerosol that further increases its ability to scatter shortwave radiation. The moisture-swelled aerosol attenuates the shortwave radiation reaching the cloud, while the longwave opacity of the moisture will diminish the cloud-top longwave cooling. All else equal, solar-induced decoupling should be reduced within the boundary layer when absorbing aerosol is present overhead, fostering a more well-mixed boundary layer. On the other hand, the reduced cloud-top longwave cooling will drive less turbulence within the boundary layer, providing the opposite feedback. Thus, the inference of the cloudy boundary-layer adjustments to free-tropospheric aerosol loadings will require knowledge of the boundary-layer decoupling. The Balloon-borne Sounding System (SONDE) data sets will be applied to assess boundary-layer decoupling throughout the annual cycle. WACR radar data will help distinguish the impact of turbulent mixing from microphysics upon the spectrum width (e.g., Fang et al. 2012). The evolution of the boundary layer will also be characterized using a new AERI-based retrieval that can infer temperature and humidity profiles at high time resolution from both clear and cloudy-sky scenes (Turner et al., 2014).

A vertical profile of aerosol extinction can be inferred from the lidar backscattered intensity using AERONET or other aerosol optical depths as a constraint. The SSA will be determined from the surface aerosol measurements and assumed to represent the entire column. The cloud optical depth can be inferred from NFOV or sun photometer zenith radiance measurements (Chiu et al. 2012). From these inputs, estimates of the aerosol heating rates can then be calculated. When clouds are inhomogeneous, radiative transfer results can be filtered for spectrally consistent data that can be compared to SASZE and SASHE measurements, similar to what has been done with an aircraft-based solar spectral flux radiometer (Kindel et al. 2011).

When the aerosols are embedded within the cloud layer, a similar statistical combination of modeling and measurements can quantify the heating rates (Schmidt et al. 2009). Competing radiative impacts from changes in microphysics and cloud spatial organization can be discriminated using three-dimensional radiative transfer modeling of large-eddy simulations initialized by the observations and compared to measured irradiances (Zuidema et al. 2008; Schmidt et al. 2009). Such radiative closure provides a means of not only assessing retrieval accuracy, but also for extrapolating local observations with confidence to larger scales. This represents a significant opportunity for satellite retrieval development and assessment within a difficult space-based remote sensing regime.

3.4 Distinguishing Aerosol from Meteorological Effects (H2, H4)

A first-order activity is to understand the depth and complexity of the well-coupled aerosol-meteorological state. It is imperative that the meteorology be well characterized, towards constraining modeling simulations and confidently distinguishing aerosol effects. As much will be done prior to the campaign as possible. Burning over continental Africa occurs throughout the full year, but the circulation pattern that favors the westward advection of the aerosol occurs primarily between July and November, and is most pronounced in September-October. At this time the aerosol-bearing southerly African easterly jet (Jackson et al. 2009), centered at approximately 100 S, or near the latitude of Ascension Island, is most pronounced (Adebisi and Zuidema 2016). This outflow is accompanied by moisture that also influences the cloudy boundary layer. Boundary-layer clouds are known to be highly influenced by boundary-layer conditions prevailing 24-36 hours upstream (e.g., Klein et al. 1997; Mauger and Norris 2007), which for Ascension Island occurs southeast of the island. Thus, unlike the southeastern Pacific, a strong wind shear exists between the free-tropospheric and boundary-layer winds (compare, e.g., Figure 1 with Figure 3).

The meteorological conditions encouraging aerosol outflow and their dynamical impact on the low cloud fields will be characterized using daily ERA-Interim reanalyses (e.g., Adebisi et al. 2015), with the goal of defining an easy-to-apply meteorological metric associated with the aerosol outflow (e.g., the strength of the southerly African easterly jet; Adebisi and Zuidema 2016). Thermodynamic observations of the entire annual cycle (Figure 7) confirm that large-scale conditions at Ascension Island are consistently representative of the trade-wind conditions, easing the ability to identify smoky and pristine large-scale conditions with similar thermodynamic context at Ascension. The natural variability of the low cloud fields at Ascension will be examined using satellite data as a function of both the aerosol-associated meteorological metric and the cloud upwind conditions as defined by reanalysis data sets prior to the campaign. The four-times-daily soundings, increasing to eight times daily during the August-September IOP, combined with a RWP, will characterize Ascension Island's wind vertical profile and can help fine-tune the analysis begun with ERA-Interim data sets. UK Met Office measurements at St. Helena Island, which is upstream of Ascension if considering the boundary-layer winds, but downstream if considering the free-tropospheric winds driving the aerosol outflow, will be related to the ARM measurements at Ascension Island.

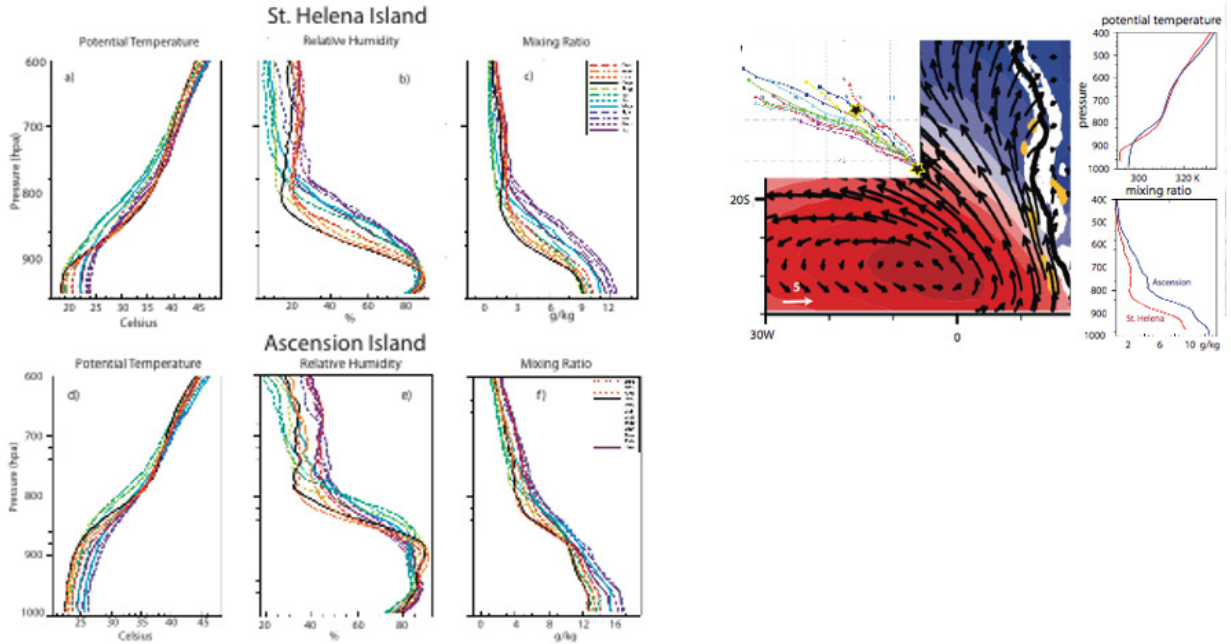


Figure 7. a)-g) Monthly-mean profiles of atmospheric potential temperature, relative humidity, and mixing ratio clearly highlight the warmer, deeper, and moister boundary layer at Ascension Island (bottom row) compared to St. Helena (top row), and the distinct seasonal cycle at each location. From 2000-2012 Integrated Global Radiosonde Archive (IGRA) soundings (radiosondes were discontinued at Ascension Island after 2012). Right panel: September-October ERA-Interim 1000 hPa climatological winds and sea level pressure with an ensemble of September 2013 Hybrid Single-Particle Lagrangian Integrated Trajectory (HYSPLIT) forward trajectories from St. Helena Island (superimposed) passing near Ascension Island, and September-mean thermodynamic profiles from both islands.

3.5 Measurements that Span the Full Annual Cycle and Low Cloud Model Parameterization Development Support (H2, H4)

The BB aerosol radiative properties will be evaluated at Ascension as a function of time during the July-November biomass burning season. Should the smoke single-scattering albedo be determined to trend systematically at the remote Ascension Island, this will also impact the radiative heating profile. The impact (and frequency) of BB aerosol entrained into the boundary layer may in turn also evolve with time, and will be evaluated. AERONET measurements from the continent and at St. Helena will help determine if and how similar systematic trends typify all of the locations.

The seasonal cycle is also an important metric with which to assess the behavior of low clouds within climate models. Many CMIP5 models exhibit a seasonal cycle in liquid water path that is out of phase with the observed seasonal cycle over the main stratocumulus deck (Figure 8) as defined within Klein and Hartmann (1993; 100-200°S, 0-100°E).

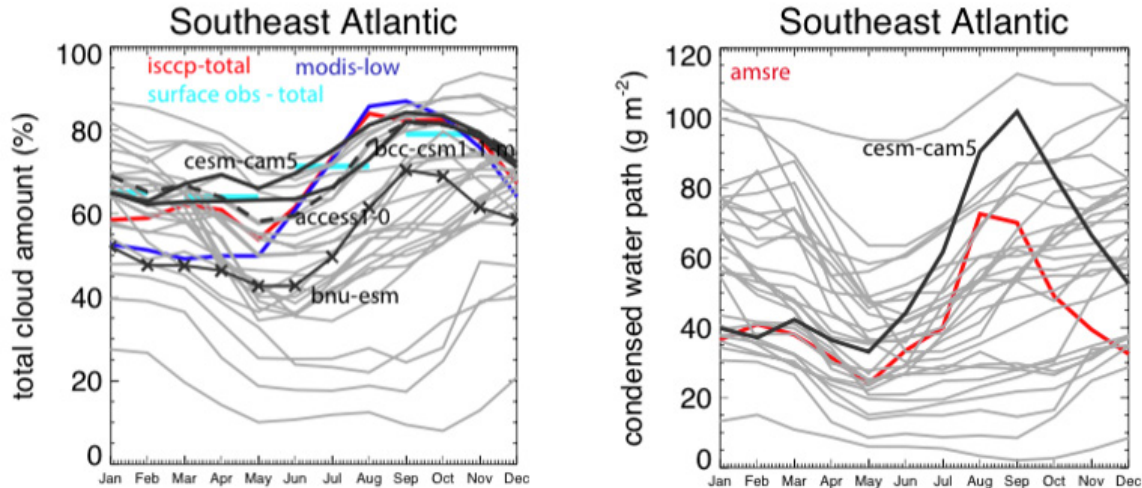


Figure 8. The annual cycle in left) cloud amount and right) liquid water path over the 100-200°S, 0-100°E region (Klein and Hartmann 1993) in Coupled Model Intercomparison Project (CMIP)5 models and observations. These include Hybrid Single-Particle Lagrangian Integrated Trajectory (ISCCP), Extended Edited Synoptic Cloud Reports Archive (EECRA), and MODIS and Advanced Microwave Scanning Radiometer-Earth Observe System (AMSR- E) (2002-2012). The black lines indicate CMIP5 models with the highest correlations to the observed values. The DOE-supported Community Earth System Model-Community Atmosphere Model (CESM-CAM5) depicts the most realistic annual cycle of the models shown, supporting further cloud parameterization activities.

Modeled skill at capturing the annual variation in low cloud fraction has been shown to increase for models with more realistic annual cycles in the lower tropospheric stability (Noda and Satoh 2014), suggesting the problem lies more with the internal cloud parameterizations than with the climate model depictions of the large-scale state. Ascension and St. Helena Island can serve as foci for more detailed output of the next-generation CMIP6 models, to further diagnose model behavior. A correct seasonal cycle in cloud fraction and cloud properties in both global aerosol models and climate models lacking aerosol representation, is a prerequisite for models seeking to further improve the internal cloud model representation. The concurrent radiosonde thermodynamic profiles combined with cloud property measurements will allow for a sensitive interrogation using a range of models, from process-level large-eddy simulations, to climate models, to further parameterization efforts for low clouds. Efforts will be made to advance modeling foci on low clouds through ensuring and developing the value-added products most useful for Climate Process Teams, the DOE Cloud-Associated Parameterizations Testbed (CAPT), and the DOE Aerosol Modeling Testbed and Large-Eddy Simulation Testbeds. The radiosondes, most particularly during the IOP when radiosondes are launched 8x/day on Ascension, along with more radiosondes launched on St. Helena by the UK Met Office, will provide crucial initialization and evaluation products.

4.0 Site Description, Planning, Value-Added Products, and Collaborations

4.1 Site Description

Ascension Island is governed as part of a larger British Overseas Territory that includes St. Helena and Tristan da Cunha. The island does not maintain a permanent population and a contract of employment is required for residence upon the island, although opportunities for tourism are becoming more available. The UK Royal Air Force and US Air Force both maintain a presence, centered on WideAwake Airfield. The US Air Force presence (~20 personnel) is an auxiliary base of Patrick Air Force Base in Florida, and the island is serviced regularly every 60 days by a US cargo ship, the *MV Ascension*, making round trips to and from Cape Canaveral, Florida. The island has a history of scientific endeavors because of its unique location. It is used as a rocket tracking station, Anglo-American signals intelligence facility, BBC World Service relay station, and hosts ground antenna that assist in the operation of the Global Positioning System. Radiosondes were launched from Ascension Island with US Government funding until 2012, but no radiosonde launchings have occurred since then. Ascension Island is still an AERONET site. The UK Met Office has used Ascension Island as a stop on its ferry flights to and from Africa (e.g., SAFARI), and some limited in situ data are available from those flights (Figure 4). On St. Helena, the UK Met Office has been launching almost daily radiosondes for many decades, archived at higher vertical resolution since 2000. The higher vertical resolution is a necessary condition for supporting research into aerosol-cloud-meteorological characterization at St. Helena (Adebisi et al. 2015). Lower-resolution radiosonde data are available for both sites through the IGRA database (Figure 7).

Ascension is a volcanic remnant with a maximum altitudes of 818 meters. Ascension does not intrude above the cloud-topped boundary layer (Figure 9), but the island is nevertheless capable of modifying the flow, primarily visible through a wake effect seen in satellite imagery (Figure 9). This should not affect the surface-based aerosol measurements of mass, composition, and absorption, but the boundary-layer flow modification could affect, for example, the mean cloud fraction and cloud diurnal cycle. The island effects will affect site location choice, and the island impact on cloudiness will need to be assessed. The TSI camera will assess local gradients in the cloud cover. A larger-range option for assessing island effects could be through Unmanned Aerial Vehicles (perhaps through DOE's guest instrumentation program), and to compare aircraft launches and departures to the radiosondes. A satellite approach would be to assess cloud retrievals from the Visible Infrared Imaging Radiometer Suite (VIIRS), available at 750 m resolution but only at regular times, combined with cloud retrievals from the diurnally resolving geostationary Spinning Enhanced Visible and Infrared Imager (SEVIRI) instrument. Such analysis is anticipated as part of the effort to distinguish meteorological effects already (see Section 3.4).

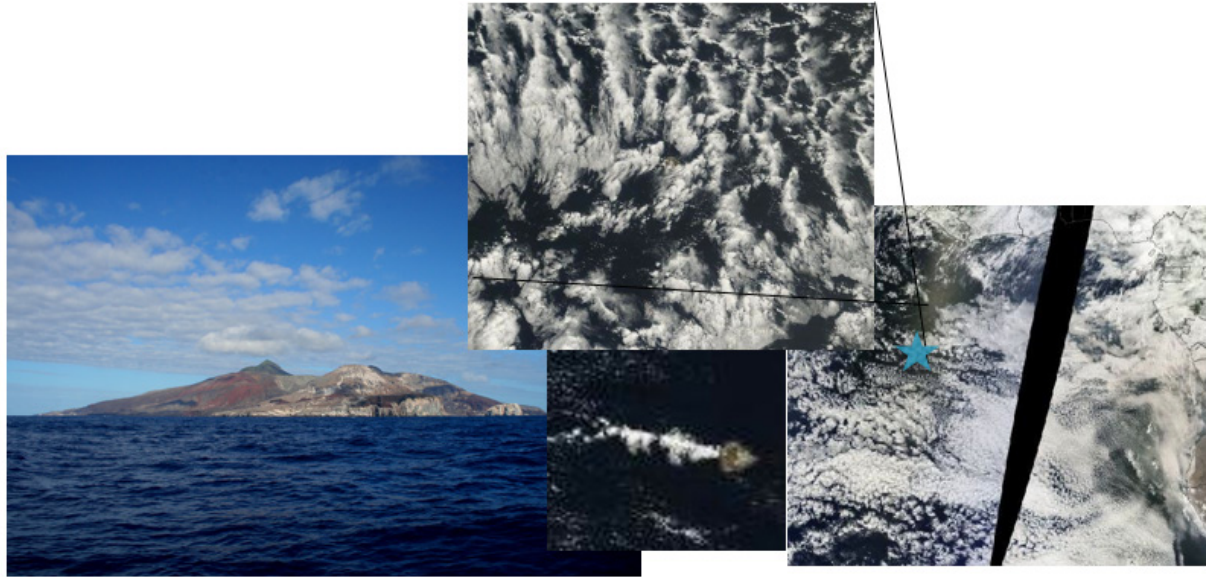


Figure 9. Leftmost panel: Ascension Island seen in profile. The rightmost panel indicates the location of Ascension within the southeast Atlantic using MODIS satellite imagery from September 4, 2013, with an expanded view centered upon Ascension (blue star) in the top middle panel. CALIOP imagery from the next day (Figure 5) indicates the presence of smoke. The bottom middle panel shows an example of the island wake effect, from September 30, 2013.

A topographic map indicating developed roads and sites, as well as the anticipated distribution of instrumentation, is included as Figure 10. The AMF1/MAOS will be located at 365 m on the windward side. Its distance from the airport and from other habitation is intended to secure aerosol measurements typical of offshore. The necessary power generator will be located as far away, downwind, from the instruments as possible. The radiosondes will be launched from the airport, adding to a previous long time series. A microwave radiometer will also be placed there, augmenting a ceilometer and an AERONET site that are already located there.

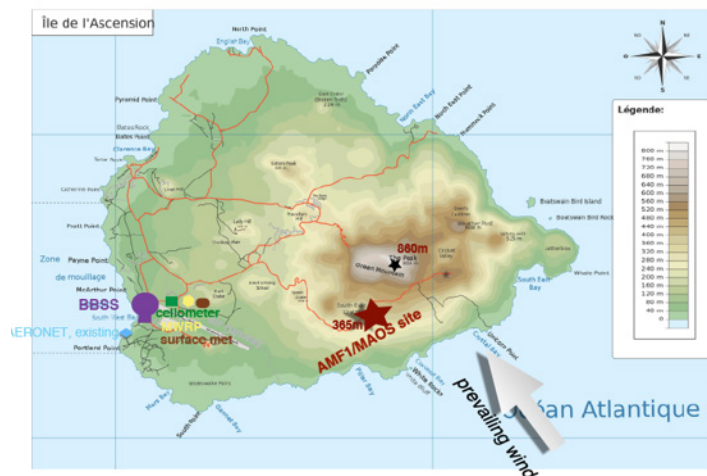


Figure 10. Ascension Island layout of instrumentation.

4.2 Related Campaigns

4.2.1 CLARIFY and ORACLES

Complementary activities were conducted by the UK Met Office and NASA. The UK Met Office Cloud-Aerosol-Radiation Interactions and Forcing: Year 2017 (CLARIFY; PI: Jim Haywood) deployment of its FAAM BAe-146 plane from Ascension spanned mid-August to mid-September of 2017. The NASA ORACLES (Observations of Aerosols above Clouds and their Interactions, PI: Jens Redemann, NASA AMES; Deputy PI: Rob Wood) is a multi-year, multi-aircraft deployment. It was based out of Walvis Bay, Namibia in September, 2016, and Sao Tome in August 2017 (and will be late September through late October, 2018). ORACLES deployed the P-3 and ER-2 planes in 2016, and the P-3 alone in 2017 and 2018. NASA also established a new AERONET site on St. Helena in 2016. The French Aerosols, Radiation and Clouds in Southern Africa (AEROCLO-Sa) campaign, (PI: Paola Formenti) deployed a Falcon plane out of Walvis Bay in August, 2017 and augmented its surface measurements in Henties Bay, Namibia.

The UK CLARIFY similarly investigated the direct, semi-direct, and indirect effects of biomass burning aerosols over the SE Atlantic. CLARIFY will focus on using its measurements to immediately improve the UK Met Office model, which has incorporated the Global Model of Aerosol Processes (GLOMAP)-mode state-of-the-science aerosol model (Mann et al. 2010; Bellouin et al. 2013). The UK suite of remote sensors will provide the upwind (boundary-layer) and downwind (free-tropospheric) information on the evolution of cloud and aerosol properties that are also being sampled at Ascension. The lead investigator, Dr. Jim Haywood, a co-investigator on LASIC, will facilitate coordination and data sharing between the projects. The unified UK Met Office operational forecast model will be applied at 4-km resolution for the campaign, with the forecasts shared between all campaigns. Post-campaign modeling exercises are anticipated to incorporate the data sets from all campaigns. Meteorological forecasts done in the context of CLARIFY will be tested with LASIC data sets.

The NASA ORACLES (Observations of Aerosols above Clouds and their Interactions, <http://espo.nasa.gov/oracles>; PI: Jens Redemann, NASA Ames Research Center; Deputy PI: Rob Wood) project will overlap with the CLARIFY campaign in 2016, during which time the NASA P-3 plane will also be based out of Walvis Bay, Namibia. ORACLES focuses on using airborne remote sensing tools that are important to future NASA satellite missions. The NASA P-3 plane will host aerosol and cloud in situ instrumentation, including a high-spectral-resolution lidar (HSRL-2), cloud radars, and solar spectral flux radiometers (SSFR and 4STAR). Most of the CLARIFY and ORACLES research flights will take place closer to the Namibian coast, both upstream (boundary layer) and downstream (free-troposphere) of the airflow encountering Ascension. ORACLES will study intraseasonal variations (August to October) in aerosol and cloud properties and their interaction, in three campaigns between 2016 and 2018. The NASA P-3 plane was supplemented by the ER-2 plane in 2016, which included remote-sensing (HSRL-2), enhanced MODIS Airborne Simulator (eMAS), Airborne multiangle spectro-polarimeter imager (AirMSPI), and an SSFR).

NASA ORACLES deployed its P-3 plane to equatorial Sao Tome Island (6.50° E), in the Gulf of Guinea, in August of 2017. This situated the plane near the aerosol exiting continental Africa, and over warmer waters encouraging deeper boundary layers, enhancing the sampling for smoke-cloud microphysical interactions. Half of the flights were devoted to survey flights along 50° E between the Equator and 15° S.

A “suitcase” brought the C-130 to Ascension Island and also allowed the plane to do some sampling of the offshore boundary layer unobstructed by the island.

A larger Scientific Coordination Group, composed of the principal investigators and other major personnel, optimized the coordination between the different campaigns. Another possibly complementary science project is the NASA Atmospheric Tomography Mission (PI: Steve Wofsy, Harvard), which undertook/is undertaking four around-the-world research flights in five years with stops in Ascension to understand the chemical processes controlling methane and ozone. A ground station of the Total Carbon Column Observing Network measures all the major greenhouse gases, described at https://tccon-wiki-caltech.edu/Sites/Ascension_Island (PI: Dietrich Feist, Max Planck Institute-Biogeochemistry).

4.2.2 The LASIC SSA Constraint Study

The intrinsic radiative property of smoke supporting the absorption, or the SSA, varies with composition, aging, and hygroscopicity. The SSA is still poorly constrained for smoke emanating from African continental fires after long-range transport. Filter-based techniques such as the PSAP, nephelometers, and aethalometers estimate extinction from the change in light transmission through particle-imbibed filters. The cavity-attenuated phase shift (CAPS)-SSA uses an entirely different approach. It employs a unique optical design to simultaneously measure aerosol light extinction and scattering in the same sample volume. These can then be used to derive the SSA and aerosol absorption. The CAPS-SSA absorption estimate will serve as a reference and anchor for the longer-term filter-based measurements, helping to fulfill an important goal of the LASIC campaign and of the Atmospheric System Research (ASR) Aerosol Working Group. This endeavor is a joint effort between Aerodyne and ARM, and brought the CAPS-SSA monitor out to Ascension from August through September in 2017.

4.2.3 Supplemental Measures for the LASIC Campaign

Supplementary measurements were desired for the LASIC campaign to properly characterize the representativeness of the chosen AMF1/MAOS site, to address the island effect, and to co-locate a microwave radiometer at the radiosonde launch site, towards properly constraining the radiosonde humidity profiles.

5.0 Highlights

The smokiest day of the 17-month campaign, recorded at the surface by the single-particle soot photometer, occurred on August 13, when the daily mean black carbon mass concentration almost reached 1700 ng m^{-3} . As described in Zuidema et al. (2018), on 13 August, 2016, closed-cell cumulus clusters with cores reaching 2 km generated upper-level stratiform cloud, with lower local orographically lifted cloud at the AMF1 site fully attenuating the lidar signal. The following day was characterized by more suppressed wind-aligned shallow cumuli that allowed the micropulse lidar to more fully probe the atmosphere. Smoke was present to above 3 km (Figure 11a, encompassing 14 August 12 UTC to 16 August 00 UTC). At times, the smoke within the boundary layer almost fully extinguishes the lidar signal (e.g., 14 August 15 UTC), and the ceilometer-derived cloud base heights are included to distinguish aerosol from cloud. The pronounced extinctions coincide with relative humidity maxima, one at approximately 800 m, corresponding to the lifting condensation level, and 1.5 km just below the trade-wind inversion (Figure 11c). These relative humidity profiles indicate a decoupled boundary layer, often

observed at Ascension. Both cloud-containing layers are individually well mixed in moisture (not shown, but consistent with the linear increase in the relative humidity with altitude). The deliquescence of the smoke particles is confirmed by the lower lidar volume depolarization ratios within the boundary layer (Figure 11b) indicative of more spherical particles.

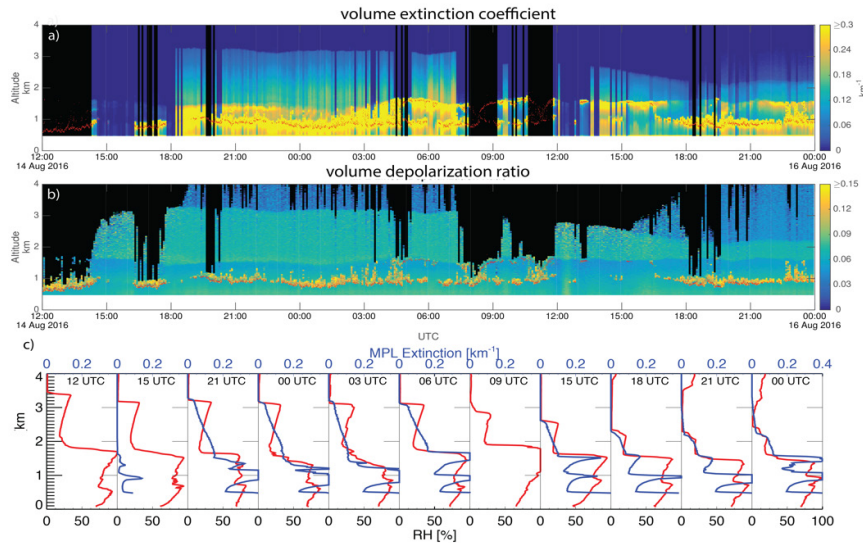


Figure 11. 14 August 1200 UTC-16 August 00 UTC time series of the micropulse-lidar-derived a) volume extinction coefficient, and b) volume depolarization ratio, both with ceilometer-derived cloud bases shown in red, and c) radiosonde profiles of relative humidity (red) and lidar volume extinction coefficients (blue). The lidar is located at 365 m elevation while the radiosondes are launched approximately 5 km away at the airport near sea level, in generally drier conditions below 1 km.

The near-surface water vapor mixing ratio of 12-14 g kg⁻¹ decreases to ~ 3 g kg⁻¹ above the trade-wind inversion (not shown) for a relative humidity of 20-30%. The specific humidity of the upper aerosol layer indicates air that was last saturated at an altitude of approximately 5 km, consistent with the residual of a deep continental boundary layer. The lidar volume depolarization ratio increases, consistent with more desiccated, aspherical aerosol. The higher aerosol layer is resting directly upon the trade-wind inversion, most obviously in Fig. 11c; this feature was common to almost all the days with an upper-level smoke layer (visually determined from daily lidar imagery). The lidar extinction values above the cloud layer are considered biased low by a factor of 0.35 and the vertical gradient in extinction reflects attenuation of the lidar signal, as the moisture layer is well mixed. Either by assuming the extinction just above the cloud layer of 0.1 km⁻¹ is a constant through the aerosol layer, or by correcting by a factor of 2.8, supports an estimate for the above-cloud aerosol optical depth of approximately 0.2 until mid-day 15 August, or almost one-half of the column sun-photometer-derived aerosol optical depth of 0.48 between 15-18 UTC on 14 August.

Radiosonde-derived wind profiles indicate westward winds throughout the entire 0-4-km column during 13-16 August, 2016 (not shown). The 7-day HYSPLIT back trajectories at 500, 1000, and 2000 m indicate a direct northwestward transport from continental African fire source regions, with the week-long meteorology integrating to bring continental smoke to Ascension Island (Figure 12). This atmospheric boundary-layer flow contrasts with the climatological wind pattern of southeasterlies advecting clean Southern Hemisphere air around the southern Atlantic subtropical anticyclone, apparent on back

trajectories for most other August days (Figure 12e). 31 August is another day with both high near-surface refractory black carbon (rBC) values and a 500-m back trajectory tracing back to continental Africa. This flow pattern, previously noted in Swap et al. (1996), is important for explaining high near-surface aerosol loadings, and can also include aerosol transported at a slightly higher altitude (~ 1 km) that becomes entrained into the boundary layer further offshore.

A further, separate, notable result from the quality-controlled filter measurements, PSAP, and the nephelometer, was that the single-scattering albedo increased systematically from August to October in both 2016 and 2017, with monthly-means of 0.78 ± 0.02 (August), 0.81 ± 0.03 (September) and 0.83 ± 0.03 (October) at the green wavelength. The increase with time is consistent with Eck et al. (2013). What was initially surprising were the values themselves, which were lower than those previously reported within Leahy et al. (2012). Filter-based techniques such as the Particle Soot Absorption Photometer (PSAP), nephelometers, and aethalometers estimate extinction from the change in light transmission through particle-imbibed filters.

The cavity-attenuated phase shift (CAPS)-SSA takes an entirely different approach. It uses a unique optical design to simultaneously measure aerosol light extinction and scattering in the same sample volume. The LASIC SSA-CONSTRAINT study, a joint effort between Aerodyne and ARM, brought a CAPS-SSA monitor to Ascension, with measurements made from August 4 to September 22, 2017. The CAPS-SSA measurements corroborate the PSAP absorption, and reported an average SSA value of 0.77 ± 0.03 that supports the filter-based SSA measurements.

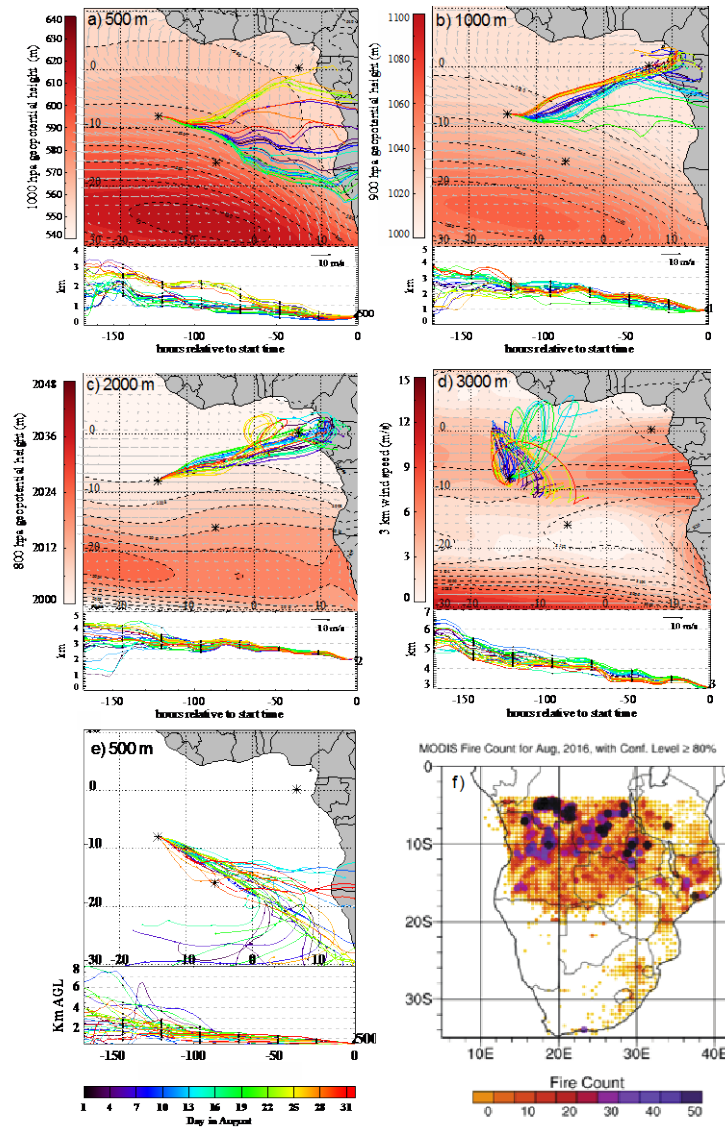


Figure 12. Twenty-seven-member ensemble HYSPLIT back trajectories initialized on 13 August 2016 12 UTC originating from Ascension Island at a) 500 m, b) 1 km, c) 2 km, and d) 3 km, driven by 0.5° NCEP GFS meteorology. The August-2016 mean ERA-Interim geopotential heights and vector winds are overlaid at a) 1000, b) 900, c) 800, and d) 700 hPa (dashed black contours, and as closed color contours on panels a-c). Panel d) indicates the 3-km wind speeds in closed color contours. e) One 500-m back trajectory per day of August (12 UTC). f) Spatial distribution of MODIS-detected fires for August of 2016.

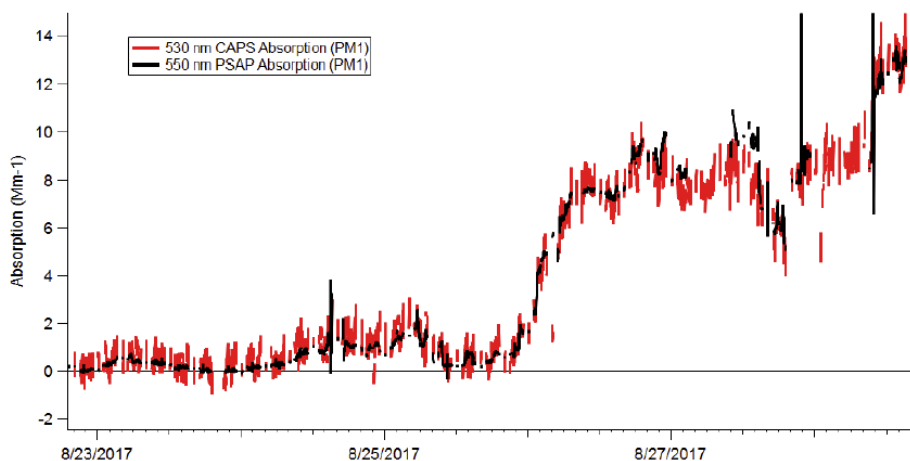


Figure 13. Cavity-attenuated phase shift (CAPS) and particle soot absorption photometer (PSAP) aerosol light absorption measurements for late August, 2016, Ascension Island. Plot courtesy of Tim Onasch.

Instrument issues. The W-band radars did not perform well, and little data are available from them. Doppler lidar data are not available for the first biomass burning season in 2016.

6.0 Results

Some initial results are shown in Zuidema et al. 2018 with its Figure 1 repeated here. The rBC mass concentrations already regularly exceed 10 ng m^{-3} by June. The variability is predominantly synoptic, with smokier and cleaner time periods able to alternate within a few days of each other. August is the smokiest month depicted, with a monthly-mean rBC mass concentration reaching almost 500 ng m^{-3} . The maximum rBC exceeded 1700 ng m^{-3} on 13 August, 2016, followed by another local maximum on 30 August. The peaks in the near-surface values are comparable to those measured closer to the African coast between 3–6 km altitude in September, 2016 by a NASA P-3 research plane. A strong subsequent decline in September occurs to much lower and even occasionally zero concentrations of black carbon.

Nevertheless, even in November rBC mass values still exceeded 3 ng m^{-3} (the SP2 detection limit) 90% of the time, although overall the monthly mean value was much lower at 32 ng m^{-3} . Few island sources exist for the black carbon, with the instrumentation located on the windward side of the island upwind from the site generator. Details of the aerosol light absorption variability with time track that of the rBC. Most of the aerosol can be activated into cloud condensation nuclei by supersaturations of 0.2%, more prominently so in June, indicating the aerosol's potential to modify clouds microphysically. A supersaturation (SS) of 0.2% is readily achieved in the marine environment (Wood et al. 2012). At 0.4% SS, all or nearly so of the condensation particles with diameters $> 10 \text{ nm}$ are activated.

The variability in the carbon monoxide (CO) values indicates that clean background conditions representative of the atmosphere above the southern high-latitude ocean, determined when the CO is at the 0.06 ppm noise floor, can also occur, sometimes within only a few days of a heavy smoke event. Also evident is that the CO:particle count ratio increases over time; the CO:rBC ratio is also lower in June than in August–September, implying that either the aerosol in June is more aged (Heald et al. 2014) or stems from more actively flaming sources producing less CO compared to smoldering fires (Liu et al. 2011).

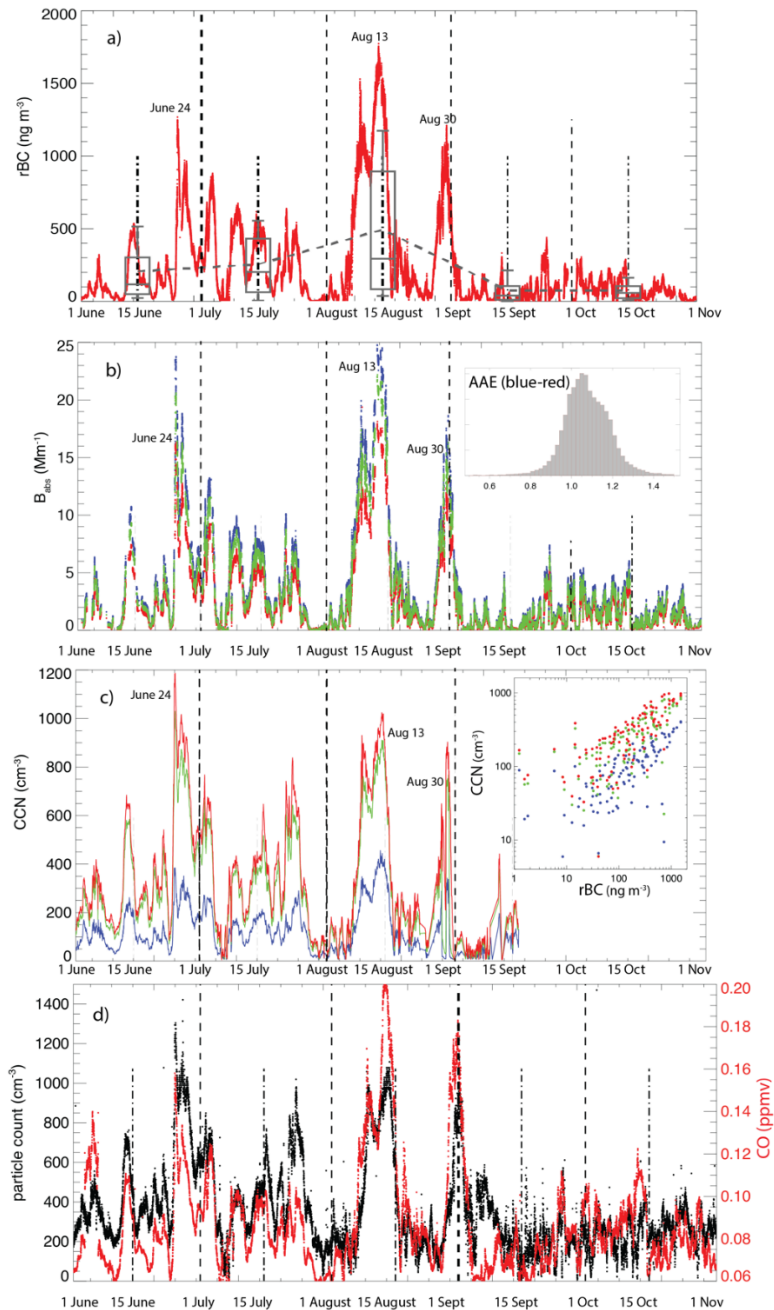


Figure 14. 1 June–31 October, 2016 time series of a) single-particle soot photometer (SP2)-derived refractory black carbon (rBC) mass concentrations. Monthly 10, 25, 50, 75, and 90 percentiles are indicated, with a dotted line connecting monthly mean values. b) Particle soot absorption photometer (PSAP) aerosol light absorption coefficients at three wavelengths (blue: 464 nm, green: 529 nm, red: 648 nm) as an average of the Virkkula1 (2010) and Ogren and Bond (2010) corrections. The inset indicates the relative frequency distribution of the blue-red absorption Angstrom exponent, only calculated when the blue nephelometer-derived scattering $> 10 \text{ Mm}^{-1}$. c) Cloud condensation concentrations (CCN) at 0.1%, 0.2%, and 0.4% supersaturations (data from 15 September to 1 November are missing). Inset indicates daily averaged CCN versus rBC mass concentrations. d) Condensation particle concentrations (black; minimum particle diameter of 10 nm) and carbon monoxide (red).

7.0 Public Outreach

The LASIC campaign is advertised through the URL <https://www.arm.gov/research/campaigns/amf2016lasic>. It has most recently been highlighted in the ARM March, 2018 newsletter.

8.0 LASIC Publications

Selected early findings mentioned under “Results” are now published in Zuidema et al. 2018. LASIC presentations have been made at the American Geophysical Union (AGU) annual meeting (2016 and 2017) by Allison Aiken, Sam Pennypacker, and Rob Wood, and Jianhao Zhang, Rodrigo Delgadillo, and Paquita Zuidema. The annual DOE ASR 2016 and 2017 meetings included LASIC-specific breakout sessions with presentations by, in addition to those mentioned above, Yann Blanchard and Christine Chiu, Art Sedlacek, Stephen Springston, Connor Flynn, Tim Onasch, and Yang Fen.

8.1 Journal Articles/Manuscripts

Zuidema, P, A Sedlacek, C Flynn, S Springston, R Delgadillo, J Zhang, A Aiken, and P Muradyan. 2018. “The Ascension Island boundary layer in the remote southeast Atlantic is often smoky.” *Geophysical Research Letters* doi:[10.1002/2017GL076926](https://doi.org/10.1002/2017GL076926)

8.2 Meeting Abstracts/Presentations/Posters

From the DOE ASR 2018 LASIC-focused breakout session:

1. Allison Aiken: Ambient aerosols in both smoky and reference conditions
2. Art Sedlacek: Refractory black carbon
3. Tim Onasch: LASIC CAPS measurements
4. Connor Flynn: Perspectives on filter-based derived SSA values
5. Yan Feng: Meteorological influences on biomass burning aerosol long-range transport: Observations versus CAM5 simulations
6. Yann Blanchard: Cloud properties from zenith-pointing and scanning cloud radars: Statistics and implications
7. Ewan O’Connor: Inferences on turbulence from the Doppler lidar
8. Rob Wood: Ultra-clean conditions at Ascension
9. Laura Riihimaki: Update on VAP status
10. Tak Yamaguchi: Perspectives on absorbing-aerosol-cloud interactions gained from recent modeling studies
11. Xiaohong Liu: WRF-Chem simulations of the southeast Atlantic
12. Zuidema/Saide: A community model-observational intercomparison project+assessment of WRF-CAM5 simulations using LASIC data.

9.0 References

- Abel, SJ, JM Haywood, EJ Highwood, J Li, and PR Buseck. 2003. "Evolution of biomass burning aerosol properties from an agricultural fire in southern Africa." *Geophysical Research Letters* 30(15): 1783, [doi:10.1029/2003GL017342](https://doi.org/10.1029/2003GL017342).
- Abel, S, EJ Highwood, J Haywood, and M Stringer, 2005. "The direct radiative effect of biomass burning aerosol over southern Africa." *Atmospheric Chemistry and Physics* 5(7): 1999-2018, [doi:10.1029/2005-5-1999](https://doi.org/10.1029/2005-5-1999).
- Ackerman, AS, OB Toon, DE Stevens, AJ Heymsfield, V Ramanathan, and EJ Welton. 2000. "Reduction of tropical cloudiness by soot." *Science* 288(5468): 1042-1047, [doi:10.1126/science.288.5468.1042](https://doi.org/10.1126/science.288.5468.1042).
- Adebisi, A, P Zuidema, and S Abel. 2015. "The convolution of dynamics and moisture with the presence of shortwave absorbing aerosols over the southeast Atlantic." *Journal of Climate* 28(5): 1997-2024, [doi:10.1175/JCLI-D-14-00351.2](https://doi.org/10.1175/JCLI-D-14-00351.2).
- Adebisi, A, and P Zuidema. 2016. "The role of the southern African easterly jet in modifying the southeast Atlantic aerosol and cloud environments." *Quarterly Journal of the Royal Meteorological Society* 142(697): 1574-1589, [doi:10.1002/qj.2765](https://doi.org/10.1002/qj.2765).
- Akagi, SK, JS Craven, JW Taylor, GR McMeeking, RJ Yokelson, IR Burling, SP Urbanski, CE Wold, JH Seinfeld, H Coe, MJ Alvarado, and DR Weise. 2012. "Evolution of trace gases and particles emitted by a chaparral fire in California." *Atmospheric Chemistry and Physics* 12(3): 1397-1421, [doi:10.5194/acp-12-1397-2012](https://doi.org/10.5194/acp-12-1397-2012).
- Alvarado, MJ, CR Lonsdale, RJ Yokelson, SK Akagi, H Coe, JS Craven, EV Fischer, GR McMeeking, JH Seinfeld, T Soni, JW Taylor, DR Weise, and CE Wold. 2014. "Investigating the links between ozone and organic aerosol chemistry in a biomass burning plume from a prescribed fire in California chaparral." *Atmospheric Chemistry and Physics* 15(12): 6667-6688, [doi:10.5194/acp-15-6667-2015](https://doi.org/10.5194/acp-15-6667-2015).
- Alvarado, MJ, and RG Prinn. 2000. "Formation of ozone and growth of aerosols in young smoke plumes from biomass burning: 1. Lagrangian parcel studies." *Journal of Geophysical Research – Atmospheres* 114(D9): D09306, [doi:10.1029/2008JD011144](https://doi.org/10.1029/2008JD011144).
- Andreae, MO, and D Rosenfeld. 2008. "Aerosol-cloud- precipitation interactions. Part 1. The nature and sources of cloud-active aerosols." *Earth Science Review* 89(1-2): 13-41, [doi:10.1016/j.earscirev.2008.03.001](https://doi.org/10.1016/j.earscirev.2008.03.001).
- Bellouin, N; GW Mann, MT Woodhouse, C Johnson, KS Carslaw, and M Dalvi. 2013. "Impact of the modal aerosol scheme GLOMAP-mode on aerosol forcing in the Hadley Centre Global Environmental Model." *Atmospheric Chemistry and Physics* 13(6): 3027-3044. [doi: 10.5194/acp-13-3027-2013](https://doi.org/10.5194/acp-13-3027-2013),
- Bennartz, R. 2007. "Global assessment of marine boundary layer cloud droplet number concentration from satellite." *Journal of Geophysical Research – Atmospheres* 112(D2): D02201, [doi:10.1029/2006JD007547](https://doi.org/10.1029/2006JD007547).
- Bond, TC, SJ Doherty, DW Fahey, PM Forster, T Berntsen, BJ DeAngelo, MG Flanner, S Ghan, B Karcher, D Kock, S Kinne, Y Kondo, PK Quinn, MC Sarofim, MG Schultz, M Schulz,

C Venkataraman, H Zhang, S Zhang, N Nellouin, SK Guttikunda, PK Hopke, MZ Jacobson, JW Kaiser, Z Klimont, U Lohmann, JP Schwarz, D Shindell, T Storelvmo, SG Warren, and CS Zender. 2013. “Bounding the role of black carbon in the climate system: A scientific assessment.” *Journal of Geophysical Research – Atmospheres* 118(11): 5380-5552. [doi:10.1002/jgrd.50171](https://doi.org/10.1002/jgrd.50171).

Borque, P, P Kollias and S Giangrande. 2014. “First Observations of Tracking Clouds Using Scanning ARM Cloud Radars.” *Journal of Applied Meteorology and Climatology* (53(12): 2732-22746, [doi:10.1175/JAMC-D-13-0182.1](https://doi.org/10.1175/JAMC-D-13-0182.1).

Boucher, O., D. Randall, P. Artaxo, C. Bretherton, G. Feingold, P. Forster, V.-M. Kerminen, Y. Kondo, H. Liao, U. Lohmann, P. Rasch, S. K. Satheesh, S. Sherwood, B. Stevens and X. Y. Zhang. 2013. “Clouds and Aerosols.” In *Climate Change 2013: The Physical Science Basis. Working Group I Contribution to the Fifth Assessment Report of the Intergovernmental Panel on Climate Change*, Cambridge University Press, Cambridge and New York, pp. 571-658.

Brioude, J, OR Cooper, G Feingold, M Trainer, SR Freitas, D Kowal, JK Ayers, E Prins, P Minnis, SA McKeen, GJ Frost, and E-Y Hsie. 2009. “Effect of biomass burning on marine stratocumulus clouds off of the Californian coast.” *Atmospheric Chemistry and Physics* 9: 8841-8856, [doi:10.5194/acp-10-8841-2010](https://doi.org/10.5194/acp-10-8841-2010).

Brioude, J, WM Angevine, R Ahmadov, SW Kim, S Evan, SA McKeen, E-Y Hsie, GJ Frost, JA Neuman, IB Pollack, J Peischl, TB Ryerson, J Holloway, SS Brown, JB Nowak, JM Roberts, SC Wofsy, GW Santoni, T Oda, and M Trainer. 2013. “Top-down estimate of surface flux in the Los Angeles Basin using a mesoscale inverse modeling technique: assessing anthropogenic emissions of CO, NO_x and CO₂ and their impacts.” *Atmospheric Chemistry and Physics* 13(7): 3661-3677, [doi:10.5194/acp-13-3661-2013](https://doi.org/10.5194/acp-13-3661-2013).

Chand, D, R Wood, TL Anderson, SK Satheesh, and R. Charlson. 2009. “Satellite-derived direct radiative effect of aerosols dependent on cloud cover.” *Nature Geoscience*, [doi:10.1038/ngeo0437](https://doi.org/10.1038/ngeo0437).

Chiu, C, A Marshak, C-H Huang, T Varnai, RJ Hogan, D Giles, B Holben, E O’Connor, Y Knyazikhin and W Wiscombe. 2012. “Cloud droplet size and liquid water path retrievals from zenith radiance measurements: examples from the Atmospheric Radiation Measurement Program and the Aerosol Robotic Network.” *Atmospheric Chemistry and Physics* 12(21): 10313-10329, [doi:10.5194/acp-12-10313-2012](https://doi.org/10.5194/acp-12-10313-2012).

Costantino, L, and F-M Bre’ on. 2010. “Analysis of aerosol-cloud interaction from multi-sensor satellite observations.” *Geophysical Research Letters* 37(11): L11801, [doi:10.1029/2009GL041828](https://doi.org/10.1029/2009GL041828).

Costantino, L, and F-M Bre’ on. 2013. “Aerosol indirect effect on warm clouds over South-East Atlantic, from co-located MODIS and CALIPSO observations.” *Atmospheric Chemistry and Physics* 13(1): 69-88, [doi:10.5194/acp-13-69-2013](https://doi.org/10.5194/acp-13-69-2013).

de Graaf, M, LG Tilstra, P Wang, and P Stammes. 2012. “Retrieval of the aerosol direct radiative effect over clouds from spaceborne spectrometry.” *Journal of Geophysical Research – Atmospheres* 117(D7): D07207, [doi:10.1029/2011JD017160](https://doi.org/10.1029/2011JD017160).

- de Graaf, M, N Bellouin, LG Tilstra, J Haywood, and P Stammes. 2014. “Aerosol direct radiative effect of smoke over clouds over the southeast Atlantic Ocean from 2006 to 2009.” *Geophysical Research Letters* 41(21): 7723-7730, [doi:10.1002/2014GL061103](https://doi.org/10.1002/2014GL061103).
- Duynkerke, PG, SR de Roode, MC van Zanten, J Calvo, J Cuxart, S Cheinet, A Chlond, H Grenier, PJ Jonker, M Kohler, G Lenderink, D Lewellen, C-L Lappen AP Lock, C-H Moeng, F Muller, D Olmeda, J-M Piriou, E Sanchez, and I Sednev. 2004. “Observations and numerical simulations of the diurnal cycle of the EUROCS stratocumulus case.” *Quarterly Journal of the Royal Meteorological Society* 130(604): 3269-3296, [doi:10.1256/qj.03.139](https://doi.org/10.1256/qj.03.139).
- Eck, TF, BN Holben, JS Reid, MM Mukelabai, SJ Piketh, O Torres, HT Jethva, EJ Hyer, DE Ward, O Dubovik, A Sinyuk, JS Schafer, DM Giles, M Sorokin, A Smirnov, and I Slutsker. 2013. “A seasonal trend of single scattering albedo in southern African biomass-burning particles: Implications for satellite products and estimates of emissions for the world’s largest biomass-burning source.” *Journal of Geophysical Research – Atmospheres* 118(12): 6414-6432, [doi:10.1002/jgrd.50500](https://doi.org/10.1002/jgrd.50500).
- Fang, M, RJ Doviak, and BA Albrecht. 2012. “Analytical Expressions for Doppler Spectra of Scatter from Hydrometeors Observed with a Vertically Directed Radar Beam.” *Journal of Atmospheric and Oceanic Technology* 29(4): 500-509, [doi:10.1175/JTECH-D-11-00005.1](https://doi.org/10.1175/JTECH-D-11-00005.1).
- Fast, JD, WI Gustafson Jr., EG Chapman, RC Easter, JP Rishel, RA Zaveri, GA Grell, and MC Barth. 2011. “The Aerosol Modeling Testbed: A Community Tool to Objectively Evaluate Aerosol Process Modules.” *Bulletin of the American Meteorological Society* 92(3): 343-360, [doi:10.1175/2010BAMS2868.1](https://doi.org/10.1175/2010BAMS2868.1).
- Feingold, G, H Jiang, and JY Harrington. 2005. “On smoke suppression of clouds in Amazonia.” *Geophysical Research Letters* 32(2): L02804, [doi:10.1029/2004GL021369](https://doi.org/10.1029/2004GL021369).
- Feingold, G, and H Siebert. 2009. “Cloud-aerosol interactions from the micro to the cloud scale.” In *Strungmann Forum Report*, vol. 2. MIT Press, Cambridge, Massachusetts.
- Ghan, SJ, X Liu, RC Easter, R Zaveri, PJ Rasch, J-H Yoon, and B Eaton. 2012. “Toward a Minimal Representation of Aerosols in Climate Models: Comparative Decomposition of Aerosol Direct, Semidirect, and Indirect Radiative Forcing.” *Journal of Climate* 25(19): 6461-6476, [doi:10.1175/JCLI-D-11-00650.1](https://doi.org/10.1175/JCLI-D-11-00650.1).
- Garstang, M, PD Tyson, R Swap, M Edwards, P Kållberg, and JA Lindesay. 1996. “Horizontal and vertical transport of air over southern Africa.” *Journal of Geophysical Research – Atmospheres* 101(D19): 23721-23736, [doi:10.1029/95JD00844](https://doi.org/10.1029/95JD00844).
- Granier, C, B Bessagnet, T Bond, A D’Angiola, HD van der Gon, GJ Frost, A Heil, JW Kaiser, S Kinne, Z Klimont, S Kloster, J-F Lamarque, C Lioussé, T Masui, F Meleux, A Mieville, T Ohara, J-C Raut, K Riahi, MG Schultz, SJ Smith, A Thompson, J van Aardenne, GR van der Werf, and DP van Vuuren. 2011. “Evolution of anthropogenic and biomass burning emissions of air pollutants at global and regional scales during the 1980–2010 period.” *Climatic Change* 109: 163-190, [doi: 10.1007/s10584-011-0154-1](https://doi.org/10.1007/s10584-011-0154-1).

- Hannay, C, DL Williamson, JJ Hack, JT Kiehl, JG Olson, SA Klein, CS Bretherton, and M Koehler. 2009. "Evaluation of Forecasted Southeast Pacific Stratocumulus in the NCAR, GFDL, and ECMWF Models." *Journal of Climate* 22(11): 2871-2889, [doi:10.1175/2008.JCL12479.1](https://doi.org/10.1175/2008.JCL12479.1).
- Haywood, JM, and KP Shine. 1995. "The effect of anthropogenic sulfate and soot aerosol on the clear sky planetary radiation budget." *Geophysical Research Letters* 22(5): 603-606, [doi:10.1029/95GL00075](https://doi.org/10.1029/95GL00075).
- Haywood, JM, SR Osborne, PN Francis, A Keil, P Formenti, MO Andreae, and PH Kaye. 2003. "The mean physical and optical properties of regional haze dominated by biomass burning aerosol measured from the C-130 aircraft during SAFARI 2000." *Journal of Geophysical Research – Atmospheres* 108(D13): 8473, [doi:10.1029/2002JD002226](https://doi.org/10.1029/2002JD002226).
- Haywood, JM, SR Osborne, and SJ Abel. 2004. "The effect of overlying absorbing aerosol layers on remote sensing retrievals of cloud effective radius and cloud optical depth." *Quarterly Journal of the Royal Meteorological Society* 130(598): 779-800, [doi:10.1256/qj.03.100](https://doi.org/10.1256/qj.03.100).
- Hill, AA, and S Dobie. 2008. "The impact of aerosols on non-precipitating stratocumulus. II: The semi-direct effect." *Quarterly Journal of the Royal Meteorological Society* 134: 155-165, [doi:10.1002/qj.277](https://doi.org/10.1002/qj.277).
- Hobbs, PV, P Sinha, RJ Yokelson, TJ Christian, DR Blake, S Gao, TW Kirchstetter, T Novakov, and P Pilewskie. 2003. "Evolution of gases and particles from a savanna fire in South Africa." *Journal of Geophysical Research – Atmospheres* 108(D13): 8485, [doi:10.1029/2002JD002352](https://doi.org/10.1029/2002JD002352), [D13](#).
- Holben, BN, D Tanre, A Smirnov, TF Eck, I Slutsker, N Abuhassan, WW Newcomb, JS Schafer, B Chatenet, F Lavenu, YJ Kaufman, J Vande Castle, A Setzer, B Markham, D Clark, R Frouin, R Halthore, A Karneli, NT O'Neill, C Pietras, RT Pinker, K Voss, and G Zibordi. 2001. "An emerging ground-based aerosol climatology: Aerosol optical depth from AERONET." *Journal of Geophysical Research – Atmospheres* 106(D11): 12067-12097, [doi:10.1029/2001JD900014](https://doi.org/10.1029/2001JD900014).
- IPCC. 2013. *Climate Change 2013: The Physical Science Basis. Working Group I Contribution to the Fifth Assessment Report of the Intergovernmental Panel on Climate Change*, Cambridge University Press, Cambridge and New York.
- Johnson, B, K Shine, and PM Forster. 2004. "The semi-direct aerosol effect: Impact of absorbing aerosols on marine stratocumulus." *Quarterly Journal of the Royal Meteorological Society* 130(599): 1407-1422, [doi:10.1256/qj.03.61](https://doi.org/10.1256/qj.03.61).
- Johnson, BT. 2005. "Large-eddy simulations of the semidirect aerosol effect in shallow cumulus regimes." *Journal of Geophysical Research – Atmospheres* 110(D14): D14206, [doi:10.1029/2004JD005601](https://doi.org/10.1029/2004JD005601).
- Kassianov, EI, CJ Flynn, TP Ackerman, and JC Barnard. 2007. "Aerosol single-scattering albedo and asymmetry parameter from MFRSR observations during the ARM Aerosol IOP 2003." *Atmospheric Chemistry and Physics* 7(12): 3341-3351, [doi:10.5194/acp-7-3341-2007](https://doi.org/10.5194/acp-7-3341-2007).
- Kazil, J, H Wang, G Feingold, AD Clarke, JR Snider, and AR Bandy. 2011. "Modeling chemical and aerosol processes in the transition from closed to open cells during VOCALS-Rex." *Atmospheric Chemistry and Physics* 11(15): 7491-7514, [doi:10.5194/acp-11-7491-2011](https://doi.org/10.5194/acp-11-7491-2011).

- Klein, SA, and DL Hartmann. 1993. "The seasonal cycle of low stratiform clouds." *Journal of Climate* 6(8): 1587-1606, [doi:10.1175/1520-0442\(1993\)006<1587:TSCOLS>2.0.CO;2](https://doi.org/10.1175/1520-0442(1993)006<1587:TSCOLS>2.0.CO;2).
- Klein, SA. 1997. "Synoptic variability of low-cloud properties and meteorological parameters in the subtropical trade wind boundary layer." *Journal of Climate* 10(8): 2018-2039, [doi:10.1175/1520-0442\(1997\)010<2018:SVOLCP>2.0.CO;2](https://doi.org/10.1175/1520-0442(1997)010<2018:SVOLCP>2.0.CO;2).
- Kindel, BC, P Pilewskie, KS Schmidt, O Coddington, and MD King. 2011. "Solar spectral absorption by marine stratus clouds: Measurements and modeling." *Journal of Geophysical Research – Atmospheres* 116(D10): D10203, [doi:10.1029/2010JD015071](https://doi.org/10.1029/2010JD015071).
- Kinne, S, D O'Donnel, P Stier, S Kloster, K Zhang, H Schmidt, S Rast, M Giorgetta, TF Eck, and B Stevens. 2013. "MAC-v1: A new global aerosol climatology for climate studies." *Journal of Advances in Modeling Earth Systems* 5(4): 704-740, [doi:10.1002/jame.20035](https://doi.org/10.1002/jame.20035).
- Koch, D, and AD Del Genio. 2010. "Black carbon semi-direct effects on cloud cover: Review and synthesis." *Atmospheric Chemistry and Physics* 10(16): 7685-7696, [doi:10.5194/acp-10-7685-2010](https://doi.org/10.5194/acp-10-7685-2010).
- Koffi, B, M Schulz, F-M Breon, J Griesfeller, D Winker, Y Balkanski, S Bauer, T Berntsen, M Chin, WD Collins, F Dentener, T Diehl, R Easter, S Ghan, P Ginoux, S Gong, LW Horowitz, T Iversen, A Kirkevag, D Koch, M Krol, G Myhre, P Stier, and T Takemura. 2012. "Application of the CALIOP layer product to evaluate the vertical distribution of aerosols estimated by global models: AeroCom phase I results." *Journal of Geophysical Research – Atmospheres* 117: D10201, [doi:10.1029/2011JD016858](https://doi.org/10.1029/2011JD016858).
- Kollias, P, J Remillard, E Luke, and W Szyrmer. 2011a. "Cloud radar Doppler spectra in drizzling stratiform clouds: 1. Forward modeling and remote sensing applications." *Journal of Geophysical Research – Atmospheres* 116(D13): D13201, [doi:10.1029/2010JD015237](https://doi.org/10.1029/2010JD015237).
- Kollias P, W Szyrmer, J Remillard, and E Luke. 2011b. "Cloud radar Doppler spectra in drizzling stratiform clouds: 2. Observations and microphysical modeling of drizzle evolution." *Journal of Geophysical Research – Atmospheres* 116(D13): D13203, [doi:10.1029/2010JD015238](https://doi.org/10.1029/2010JD015238).
- Kollias, P, N Bharadwaj, K Widener, I Jo, and K Johnson. 2014a. "Scanning ARM Cloud Radars. Part I: Operational Sampling Strategies." *Journal of Atmospheric and Oceanic Technology* 31(3): 569-582, [doi:10.1175/JTECH-D-13-00044.1](https://doi.org/10.1175/JTECH-D-13-00044.1).
- Kollias, P, I Jo, P Borque, A Tatarevic, and K Lamer. 2014b. "Scanning ARM Cloud Radars. Part II: Data Quality Control and Processing." *Journal of Atmospheric and Oceanic Technology* 31(3): 583-598, [doi:10.1175/JTECH-D-13-00045.1](https://doi.org/10.1175/JTECH-D-13-00045.1).
- Koren, I, YJ Kaufman, LA Remer, JV Martins. 2004. "Measurement of the effect of Amazon smoke on inhibition of cloud formation." *Science* 303(5662): 1342-1345, [doi:10.1126/Science.1089424](https://doi.org/10.1126/Science.1089424).
- Lamer, K, A Tatarevic, I Jo, and P Kollias. 2014. "Evaluation of gridded scanning ARM cloud radar reflectivity observations and vertical Doppler velocity retrievals." *Atmospheric Measurement Techniques* 7(4): 1089-1103, [doi:10.5194/amt-7-1089-2014](https://doi.org/10.5194/amt-7-1089-2014).

- Lee, S-S, G Feingold, and PY Chuang. 2012. "Effect of Aerosol on Cloud-Environment Interactions in Trade Cumulus." *Journal of the Atmospheric Sciences* 69(12): 3607-3632, [doi:10.1175/JAS-D-12-026.1](https://doi.org/10.1175/JAS-D-12-026.1).
- Li, Z, P Zuidema, and P Zhu. 2014. "Simulated convective invigoration processes at trade wind cumulus cold pool boundaries." *Journal of the Atmospheric Sciences* 71(8): 2823-2841, [doi:10.1175/JAS-D-13-0184.1](https://doi.org/10.1175/JAS-D-13-0184.1).
- Lin, B, P Minnis, T-F Fan, Y Hu, and W Sun. 2010. "Radiation characteristics of low and high clouds in different oceanic regions observed by CERES and MODIS." *International Journal of Remote Sensing* 31(24): 6473-6492, [doi:10.1080/01431160903548005](https://doi.org/10.1080/01431160903548005).
- Liu, X, RC Easter, SJ Ghan, R Zaveri, P Rasch, X Shi, J-F Lamarque, A Gettelman, H Morrison, F Vitt, A Conley, S Park, R Neale, C Hannay, AML Ekman, P Hess, N Mahowald, W Collins, MJ Iacono, CS Bretherton, MG Flanner, and D Mitchell. 2011. "Toward a minimal representation of aerosol direct and indirect effects: Model description and evaluation." *Geoscientific Model Development Discussions* 4(4): 3485-3598, [doi:10.5194/gmdd-4-3485-2011](https://doi.org/10.5194/gmdd-4-3485-2011).
- Loeb, NG, and GL Schuster. 2008. "An observational study of the relationship between cloud, aerosol and meteorology in broken low-level cloud conditions." *Journal of Geophysical Research – Atmospheres* 113(D14): D14214, [doi:10.1029/2007JD009763](https://doi.org/10.1029/2007JD009763).
- Ma, P-L, PJ Rasch, H Wang, K Zhang, RC Easter, S Tilmes, JD Fast, X Liu, J-H Yoon, and J-F Lamarque. 2013. "The role of circulation features on black carbon transport into the Arctic in the Community Atmosphere Model version 5 (CAM5)." *Journal of Geophysical Research – Atmospheres* 118(10), 4657-4669, [doi:10.1002/jgrd.50411](https://doi.org/10.1002/jgrd.50411).
- McFarquhar, GM, S Platnick, LD Di Girolamo, H Wang, G Wind, and G Zhao. 2004. "Trade wind cumuli statistics in clean and polluted air over the Indian Ocean from in situ and remote sensing measurements." *Geophysical Research Letters* 31(21): L21105, [doi:10.1029/2004GL020412](https://doi.org/10.1029/2004GL020412).
- McFarquhar, GM, and H Wang. 2006. "Effects of aerosols on trade wind cumuli over the Indian Ocean: Model simulations." *Quarterly Journal of the Royal Meteorological Society* 132(616): 821-843, [doi:10.1256/qj.04.179](https://doi.org/10.1256/qj.04.179).
- Mann, GW, KS Carslaw, DV Spracklen, DA Ridley, PT Manktelow, MP Chipperfield, SJ Pickering, and CE Johnson. 2010. "Description and evaluation of GLOMAP-mode: a modal global aerosol microphysics model for the UKCA composition-climate model." *Geoscientific Model Development* 3(2): 519-551, [doi:10.5194/gmd-3-519-2010](https://doi.org/10.5194/gmd-3-519-2010).
- Mann, JAL, JC Chiu, RJ Hogan, EJ O'Connor, TS L'Ecuyer, THM Stein, and A Jefferson. 2013. "Aerosol impacts on drizzle properties in warm clouds from ARM Mobile Facility maritime and continental deployments." *Journal of Geophysical Research – Atmospheres* 119(7): 4136-4148, [doi:10.1002/2013JD021339](https://doi.org/10.1002/2013JD021339).
- Mauger, GS, and JR Norris. 2007. "Meteorological bias in satellite estimates of aerosol-cloud relationships." *Geophysical Research Letters* 34(16): L16824, [doi:10.1029/2007GL029952](https://doi.org/10.1029/2007GL029952).

- Mechoso, CR, R Wood, R Weller, CS Bretherton, AD Clarke, H Coe, C Fairall, JT Farrar, G Feingold, R Garreaud, C Grados, J McWilliams, SP de Szoeke, SE Yuter, P Zuidema. 2014. "Ocean-Cloud-Atmosphere-Land Interactions in the Southeastern Pacific: The VOCALS Program." *Bulletin of the American Meteorological Society* 95(3): 357-375, [doi:10.1175/BAMS-D-11-00246](https://doi.org/10.1175/BAMS-D-11-00246).
- Medeiros, B, DL Williamson, C Hannay, and J Olson. 2012. "Southeast Pacific stratocumulus in the Community Atmosphere Model." *Journal of Climate* 25(18): 6175-6192, [doi:10.1175/JCLI-D-11-00503.1](https://doi.org/10.1175/JCLI-D-11-00503.1).
- Meyer, K, S Platnick, L Oreopoulos, and D Lee. 2013. "Estimating the direct radiative effect of absorbing aerosols overlying marine boundary layer clouds in the southeast Atlantic using MODIS and CALIOP." *Journal of Geophysical Research – Atmospheres* 118(10): 4801-4815, [doi:10.1002/jgrd.50449](https://doi.org/10.1002/jgrd.50449).
- Mlawer, EJ, PD Brown, SA Clough, LC Harrison, JJ Michalsky, PW Kiedron, and T Shippert, 2000. "Comparison of spectral direct and diffuse solar irradiance measurements and calculations for cloud-free conditions." *Geophysical Research Letters* 27(17): 2653-2656, [doi:10.1029/2000GL011498](https://doi.org/10.1029/2000GL011498).
- Moeng, C-H, WR Cotton, C Bretherton, A Chlond, M Khairoutdinov, S Krueger, WS Lewellen, MK MacVean, JRM Pasquier, HA Rand, AP Siebesma, B Stevens, and RI Sykes. 1996. "Simulation of a stratocumulus-topped planetary boundary layer: Intercomparison among different numerical codes." *Bulletin of the American Meteorological Society* 77(2): 261-278, [doi:10.1175/1520-0477\(1996\)077<0261:SOASTP>2.0.CO;2](https://doi.org/10.1175/1520-0477(1996)077<0261:SOASTP>2.0.CO;2).
- Moran, K, S Pezoa, C Fairall, C Williams, T Ayers, A Brewer, S de Szoeke, and V Ghate. 2011. "A motion-stabilized W-band radar for shipboard observations of marine boundary-layer clouds." *Boundary-Layer Meteorology* 143(1): 3-24, [doi:10.1007/s10546-011-9674-5](https://doi.org/10.1007/s10546-011-9674-5).
- Myrhe, G, BH Samset, M Schulz, Y Balkanski, S Bauer, TK Berntsen, H Bian, N Bellouin, M Chin, T Diehl, RC Easter, J Feichter, SJ Ghan, D Hougustaine, T Iversen, S Kinne, A Kirkevag, J-F Lamarque, G Lin, X Liu, MT Lund, G Luo, X Ma, T van Noije, JE Penner, PJ Rasch, A Ruiz, O Seland, RB Skeie, P Stier, T Takemura, K Tsigaridis, P Wang, Z Wang, L Xu, H Yu, F Yu, J-H Yoon, K Zhang, H Zhang, and C Zhou. 2013. "Radiative forcing of the direct aerosol effect from AeroCom Phase II simulations." *Atmospheric Chemistry and Physics* 13(4): 1853-1877, [doi:10.5194/acp-13/1853-2013](https://doi.org/10.5194/acp-13/1853-2013).
- Neggers, RAJ, AP Siebesma, and T Heus. 2012. "Continuous Single-Column Model Evaluation at a Permanent Meteorological Supersite." *Bulletin of the American Meteorological Society* 93(9): 1389-1400, [doi:10.1175/BAMS-D-11-00162.1](https://doi.org/10.1175/BAMS-D-11-00162.1).
- Noda, AT, and M Satoh. 2014. "Intermodel variances of subtropical stratocumulus environments simulated in CMIP5 models." *Geophysical Research Letters* 41(21): 7754-7761, [doi:10.1002/2014GL061812](https://doi.org/10.1002/2014GL061812).
- Oktem, R, Prabhat, J Lee, A Thomas, P Zuidema, DM Romps. 2014. "Stereophotogrammetry of oceanic clouds." *Journal of Atmospheric and Oceanic Technology* 31(7): 1482-1501, [doi:10.1175/jtech-d-13-00224](https://doi.org/10.1175/jtech-d-13-00224).

- Painemal, D, and P Zuidema. 2011. "Assessment of MODIS cloud effective radius and optical thickness retrievals over the Southeast Pacific with VOCALS-REx in situ measurements." *Journal of Geophysical Research – Atmospheres* 116(D24): D24206, [doi:10.1029/2011JD016155](https://doi.org/10.1029/2011JD016155).
- Painemal D, K-M Xu, A Cheng, P Minnis, and R Palikonda. 2015. "Mean structure and diurnal cycle of Southeast Atlantic boundary layer clouds: Insights from satellite observations and multiscale modeling framework simulations." *Journal of Climate* 28(1): 324-341, [doi:10.1175/JCLI-D-14-00368.1](https://doi.org/10.1175/JCLI-D-14-00368.1).
- Painemal D, S Kato, and P Minnis. 2014. "Boundary layer regulation in the southeast Atlantic cloud microphysics during the biomass burning season as seen by the A-train satellite constellation." *Journal of Geophysical Research – Atmospheres* 119(19): 11288-11302, [doi:10.1002/2014JD022182](https://doi.org/10.1002/2014JD022182).
- Petters, JL, H Jiang, G Feingold, DL Rossiter, D Khelif, LC Sloan, and PY Chuang. 2013. "A comparative study of the response of modeled non-drizzling stratocumulus to meteorological and aerosol perturbations." *Atmospheric Chemistry and Physics* 13(5): 2507-2529, [doi:10.5194/acp-13-2507-2013](https://doi.org/10.5194/acp-13-2507-2013).
- Ramanathan, V, and G Carmichael. 2008. "Global and regional climate changes due to black carbon." *Nature Geoscience*, 1: 221-227, [doi:10.1038/ngeo156](https://doi.org/10.1038/ngeo156).
- Randles, C, and V Ramaswamy. 2010. "Direct and semi-direct impacts of absorbing biomass burning aerosol on the climate of southern Africa: A Geophysical Fluid Dynamics Laboratory GCM sensitivity study." *Atmospheric Chemistry and Physics* 10(20): 9819-9831, [doi:10.5194/acp-10-9819-2010](https://doi.org/10.5194/acp-10-9819-2010).
- Remer, LA. 2009. "Smoke above clouds." *Nature Geoscience* 2: 167-168, [doi:10.1038/ngeo456](https://doi.org/10.1038/ngeo456).
- Remillard, J, P Kollias, E Luke, and R Wood. 2012. "Marine Boundary Layer Cloud Observations in the Azores." *Journal of Climate* 25(21): 7381-7398, [doi:10.1175/JCLI-D-11-00610.1](https://doi.org/10.1175/JCLI-D-11-00610.1).
- Ross, KE, SJ Piketh, RT Brientjies, RP Burger, RJ Swap, and HJ Annegarn. 2003. "Spatial and seasonal variations in CCN distribution and the aerosol-CCN relationship over Southern Africa," *Journal of Geophysical Research – Atmospheres* 108(D13): 8481, [doi:10.1029/2002JD002384](https://doi.org/10.1029/2002JD002384).
- Russell, PB, S Kinne, and R Bergstrom. 1997. "Aerosol climate effects: Local radiative forcing and column closure experiments." *Journal of Geophysical Research – Atmospheres* 102(D8): 9397-9407, [doi:10.1029/97JD00112](https://doi.org/10.1029/97JD00112).
- Sakaeda, N, R Wood, and P Rasch. 2011. "Direct and semidirect aerosol effects of southern African biomass-burning aerosol." *Journal of Geophysical Research – Atmospheres* 116(D12): D12205, [doi:10.1029/2010JD015540](https://doi.org/10.1029/2010JD015540).
- Sandu, I, B Stevens, and R Pincus. 2010. "On the transitions in marine boundary layer clouds." *Atmospheric Chemistry and Physics* 10(5): 2377-2391, [doi:10.5194/acp-10-2377-2010](https://doi.org/10.5194/acp-10-2377-2010).
- Satheesh, SK, O Torres, LA Remer, SS Babu, V Vinoj, TF Eck, RG Kleidman, and BN Holben. 2009. "Improved assessment of aerosol absorption using OMI-MODIS joint retrieval." *Journal of Geophysical Research – Atmospheres* 114(D5): D05209, [doi:10.1029/2008JD011024](https://doi.org/10.1029/2008JD011024).

- Schmidt, KS, G Feingold, P Pilewskie, H Jiang, O Coddington, and M Wendisch. 2009. "Irradiance in polluted cumulus fields: Measured and modeled cloud-aerosol effects." *Geophysical Research Letters* 36(7): L07804, [doi:10.1029/2008GL036848](https://doi.org/10.1029/2008GL036848).
- Schmidt, KS, P Pilewskie, R Bergstrom, O Coddington, J Redemann, J Livingston, P Russell, E Bierwirth, M Wendisch, W Gore, MK Dubey, and C Mazzoleni. 2010. "A new method for deriving aerosol solar radiative forcing and its first application within MILAGRO/INTEX-B." *Atmospheric Chemistry and Physics* 10(16): 7829-7843, [doi:10.5194/acp-10-7829-2010](https://doi.org/10.5194/acp-10-7829-2010).
- Schulz, M, C Textor, S Kinne, Y Balkanski, S Bauer, T Berntsen, T Berglen, O Boucher, F Dentener, S Guibert, ISA Isaksen, T Iversen, D Koch, A Kirkevag, X Liu, V Montanaro, G Myhre, JE Penner, G Pitari, S Reddy, O Seland, P Stier, and T Takemura. 2006. "Radiative forcing by aerosols as derived from the AeroCom present-day and pre-industrial simulations." *Atmospheric Chemistry and Physics* 6(12): 5225-5246, [doi:10.5194/acp-6-5225-2006](https://doi.org/10.5194/acp-6-5225-2006).
- Seidel, FC, and C Popp. 2012. "Critical surface albedo and its implications to aerosol remote sensing." *Atmospheric Measurement Techniques* 5(7): 1653-1665, [doi:10.5194/amt-5-1653-2012](https://doi.org/10.5194/amt-5-1653-2012).
- Skamarock, WC, JB Klemp, J Dudhia, DO Gill, DM Barker, MG Duda, X-Y Huang, W Wang, and JG Powers. 2008. A description of the Advanced Research WRF Version 3. NCAR Technical Note. NCAR/TN-475+STR.
- Soden, BJ, and GA Vecchi. 2011. "The vertical distribution of cloud feedback in coupled ocean-atmosphere models." *Geophysical Research Letters* 38(12): L12704, [doi:10.1029/2011GL047632](https://doi.org/10.1029/2011GL047632).
- Sorooshian, A, G Feingold, MD Lebsock, H Jiang, and GL Stephens. 2009. "On the precipitation susceptibility of clouds to aerosol perturbations." *Geophysical Research Letters* 36(13): L13803, [doi:10.1029/2009GL038993](https://doi.org/10.1029/2009GL038993).
- Sorooshian, A, G Feingold, MD Lebsock, H Jiang, and GL Stephens. 2010. "Deconstructing the precipitation susceptibility construct: Improving methodology for aerosol-cloud-precipitation studies." *Journal of Geophysical Research – Atmospheres* 115(D17): D17201, [doi:10.1029/2009JD013426](https://doi.org/10.1029/2009JD013426).
- Stevens, B, C-H Moeng, AS Ackerman, CS Bretherton, A Chlond, S de Roode, J Edwards, J-C Golaz, H Jiang, M Khairoutdinov, MP Kirkpatrick, DC Lewellen, A Lock, F Muller, DE Stevens, E Whelan, and P Zhu. 2005. "Evaluation of large-eddy simulations via observations of nocturnal marine stratocumulus." *Monthly Weather Review* 133(6): 1443-1462, [doi:10.1175/MWR2930.1](https://doi.org/10.1175/MWR2930.1).
- Stier P, NAJ Schutgens, N Bellouin, H Bian, O Boucher, M Chin, S Ghan, N Huneeus, S Kinne, G Lin, X Ma, G Myhre, JE Penner, CA Randles, B Samset, M Schulz, T Takemura, F Yu, H Yu., and C Zhou. 2013. "Host model uncertainties in aerosol radiative forcing estimates: results from the AeroCom Prescribed intercomparison study." *Atmospheric Chemistry and Physics* 13(6): 3245-3270, [doi:10.5194/acp-13-3245-2013](https://doi.org/10.5194/acp-13-3245-2013).
- Swap, RJ, HJ Annegarn, JT Suttles, MD King, S Platnick, JL Privette, and RJ Scholes. 2003. "Africa burning: A thematic analysis of the Southern African Regional Science Initiative (SAFARI 2000)." *Journal of Geophysical Research – Atmospheres* 108(D13): 8465, [doi:10.1029/2003JD003747](https://doi.org/10.1029/2003JD003747).

- Terai, CR, R Wood, DC Leon, and P Zuidema. 2012. “Does precipitation susceptibility vary with increasing cloud thickness in marine stratocumulus?” *Atmospheric Chemistry and Physics* 12(10): 4567- 4583, [doi:10.5194/acp-12-4567-2012](https://doi.org/10.5194/acp-12-4567-2012).
- Tridon, F, A Battaglia, P Kollias, E Luke, CR Williams. 2013. “Signal Postprocessing and Reflectivity Calibration of the Atmospheric Radiation Measurement Program 915-MHz Wind Profilers.” *Journal of Atmospheric and Oceanic Technology* 30(6): 1038-1054, doi:[10.1175/JTECH-D-12-00146.1](https://doi.org/10.1175/JTECH-D-12-00146.1).
- Turner, DD, and U Loehnert. 2014. “Information content and uncertainties in thermodynamic profiles and liquid cloud properties retrieved from the ground-based Atmospheric Emitted Radiance Interferometer (AERI).” *Journal of Applied Meteorology and Climatology* 53(3): 752-771, [doi:10.1175/JAMC-D-13-0126.1](https://doi.org/10.1175/JAMC-D-13-0126.1).
- Twomey, S. 1977. “The influence of pollution on the shortwave albedo of clouds.” *Journal of the Atmospheric Sciences* 34(7): 1149-1152, [doi:10.1175/1520-0469\(1977\)034<1149:TIOPOT>2.0.CO;2](https://doi.org/10.1175/1520-0469(1977)034<1149:TIOPOT>2.0.CO;2).
- Vakkari, V, V-M Kerminen, JP Beukes, P Tiitta, PG van Zyl, M Josipovic, AD Venter, K Jaars, DR Worsnop, M Kulmala, and L Laakso. 2014. “Rapid changes in biomass burning aerosols by atmospheric oxidation.” *Geophysical Research Letters* 41(7): 2644-2651, [doi:10.1002/2014GL059396](https://doi.org/10.1002/2014GL059396).
- van der Werf, GR, JT Randerson, L Giglio, GJ Collatz, PS Kasibhatla, and AF Arellano Jr. 2006. “Interannual variability in global biomass burning emissions from 1997 to 2004.” *Atmospheric Chemistry and Physics* 6(11): 3423-3441: 3648, [doi:10.5194/acp-6-3423-2006](https://doi.org/10.5194/acp-6-3423-2006).
- van der Werf, GR, JT Randerson, L Giglio, GJ Collatz, M Mu, PS Kasibhatla, DC Morton, RS Defries, Y Jin, and TT van Leeuwen. 2010. “Global fire emissions and the contribution of deforestation, savanna, forest, agricultural and peat fires (1997-2009).” *Atmospheric Chemistry and Physics* 10(6): 11707-11735, [doi:10.5194/acp-10-11707-2010](https://doi.org/10.5194/acp-10-11707-2010).
- Voigt, A, B Stevens, S Bony, and O Boucher. 2013. “Easy Aerosol – a modeling framework to study robustness and sources of uncertainties in aerosol-induced changes of the large-scale atmospheric circulation.” wcrp-climate.org/index.php/gc-clouds-circulation-activities/gc4-clouds-initiatives/368-gc-clouds-initiative3-easy-aerosol.
- Wang, H, and G Feingold. 2009a. “Modeling mesoscale cellular structures and drizzle in marine stratocumulus. Part I: Impact of drizzle on the formation and evolution of open cells.” *Journal of the Atmospheric Sciences* 66(11): 3237-3256, [doi:10.1175/2009JAS3022.1](https://doi.org/10.1175/2009JAS3022.1).
- Wang, H, and G Feingold. 2009b. “Modeling mesoscale cellular structures and drizzle in marine stratocumulus. Part II: The microphysics and dynamics of the boundary region between open and closed cells.” *Journal of the Atmospheric Sciences* 66(11): 3257-3275, [doi:10.1175/2009JAS3120.1](https://doi.org/10.1175/2009JAS3120.1).
- Wang, H, WC Skamarock, and G Feingold. 2009. “Evaluation of scalar advection schemes in the Advanced Research WRF model using large-eddy simulations of aerosol-cloud interactions.” *Monthly Weather Review* 137(8): 2547-2558, [doi:10.1175/2009MWR2820.1](https://doi.org/10.1175/2009MWR2820.1).

- Wang, H, G Feingold, R Wood, and J Kazil. 2010. “Modelling microphysical and meteorological controls on precipitation and cloud cellular structures in Southeast Pacific stratocumulus.” *Atmospheric Chemistry and Physics* 10(13): 6347-6362, [doi:10.5194/acp-10-6347-2010](https://doi.org/10.5194/acp-10-6347-2010).
- Wang, H., RC Easter, Jr, PJ Rasch, M Wang, X Liu, SJ Ghan, Y Qian, JH Yoon, PL Ma, and V Vinoj. 2013. “Sensitivity of remote aerosol distributions to representation of cloud-aerosol interactions in a global climate model.” *Geoscientific Model Development* 6: 765-782, [doi:10.5194/gmd-6-765-2013](https://doi.org/10.5194/gmd-6-765-2013).
- Wang, H, PJ Rasch, RC Easter, B Singh, R Zhang, P-L Ma, Y Qian, SJ Ghan, and N Beagley. 2014. “Using an explicit emission tagging method in global modeling of source-receptor relationships for black carbon in the Arctic: Variations, sources, and transport pathways.” *Journal of Geophysical Research – Atmospheres* 119(22): 12888-12909, doi:[10.1002/2014JD022297](https://doi.org/10.1002/2014JD022297).
- Wang, M, S Ghan, X Liu, TS L’Ecuyer, K Zhang, H Morrison, M Ovchinnikov, R Easter, R Marchand, D Chand, Y Qian, and JE Penner. 2012. “Constraining cloud lifetime effects of aerosols using A-Train satellite observations.” *Geophysical Research Letters* 39(15): L15709, [doi:10.1029/2012GL052204](https://doi.org/10.1029/2012GL052204).
- Waquet, F, F Peers, F Ducos, P Goloub, S Platnick, J Riedi, D Tanre and F Thieuleux. 2013. “Global analysis of aerosol properties above clouds.” *Geophysical Research Letters* 40(21): 5809-5814, [doi:10.1002/2013GL057482](https://doi.org/10.1002/2013GL057482).
- Welton, EJ, JR Campbell, JD Spinhirne, and VS Scott. 2001. “Global monitoring of clouds and aerosols using a network of micro-pulse lidar systems.” In *Lidar Remote Sensing for Industry and Environmental Monitoring*, Singh, UN, T Itabe, and N Sugimoto, (eds.), *Proceedings SPIE*, 4153, 151-158, [doi:10.1117/12/417040](https://doi.org/10.1117/12/417040).
- Wen, G, A Marshak, RF Cahalan, LA Remer, and RG Kleidman. 2007. “3-D aerosol-cloud radiative interaction observed in collocated MODIS and ASTER images of cumulus cloud fields.” *Journal of Geophysical Research – Atmospheres* 112(D13): D13204, [doi:10.1029/2006JD008267](https://doi.org/10.1029/2006JD008267).
- Wilcox, EM. 2010. “Stratocumulus cloud thickening beneath layers of absorbing smoke aerosol.” *Atmospheric Chemistry and Physics* 10(23): 11769-11777, [doi:10.5194/acp-10-11769-2010](https://doi.org/10.5194/acp-10-11769-2010).
- Wilcox, EM. 2012. “Direct and semi-direct radiative forcing of smoke aerosols over clouds.” *Atmospheric Chemistry and Physics* 12(1): 139-149, [doi:10.5194/acp-12-139-2012](https://doi.org/10.5194/acp-12-139-2012), 2012.
- Wood, R. 2007. “Cancellation of aerosol indirect effects in marine stratocumulus through cloud thinning.” *Journal of the Atmospheric Sciences* 64(7): 2657-2669, [doi:10.1175/JAS3942.1](https://doi.org/10.1175/JAS3942.1).
- Wood, R, M Wyant, CS Bretherton, J Remillard, P Kollias, J Fletcher, J Stemmier, S de Szoeko, S Yuter, M Miller, D Mechem, G Tselioudis, JC Chiu, JAL Mann, EJ O’Connor, RJ Hogan, X Deng, M Miller, V Ghate, A Jefferson, Q Min, P Minnis R Palikonda, B Albrecht, E Luke, C Hannay, and Y Lin. 2015. “Clouds, Aerosol, and Precipitation in the Marine Boundary Layer: An ARM Mobile Facility Deployment.” *Bulletin of the American Meteorological Society* 96(3): 419-440, [doi:10.1175/BAMS-D-13-00180.1](https://doi.org/10.1175/BAMS-D-13-00180.1).
- Wyant, MC, CS Bretherton, A Chlond, BM Griffin, H Kitagawa, CL Lappen VE Larson, A Lock, S Park, SR de Roode, J Uchida, M Zhao, and AS Ackerman. 2007. “A single-column model intercomparison of a

heavily drizzling stratocumulus-topped boundary layer.” *Journal of Geophysical Research* 112(D24): D24204, [doi:10.1029/2007JD008536](https://doi.org/10.1029/2007JD008536).

Yang, Q, WI Gustafson Jr., JD Fast, H Wang, RC Easter, H Morrison, Y-N Lee, EG Chapman, SN Spak, and MA Mena-Carrasco. 2011. “Assessing regional scale predictions of aerosols, marine stratocumulus, and their interactions during VOCALS-REx using WRF-Chem.” *Atmospheric Chemistry and Physics* 11(23): 11951-11975, [doi:10.5194/acp-11-11951-2011](https://doi.org/10.5194/acp-11-11951-2011).

Yang, Q, WI Gustafson Jr., JD Fast, H Wang, RC Easter, M Wang, SJ Ghan, LK Berg, LR Leung, and H Morrison. 2012. “Impact of natural and anthropogenic aerosols on stratocumulus and precipitation in the Southeast Pacific: A regional modelling study using WRF-Chem.” *Atmospheric Chemistry and Physics* 12(18): 14,623-14,667, [doi:10.5194/acp-12-8777-2012](https://doi.org/10.5194/acp-12-8777-2012).

Zhang, J, and JS Reid. 2010. “A decadal regional and global trend analysis of the aerosol optical depth using data-assimilation grade over-water MODIS and Level 2 MISR aerosol products.” *Atmospheric Chemistry and Physics* 10(22): 10949-10963, [doi:10.5194/acp-10-10949-2010](https://doi.org/10.5194/acp-10-10949-2010).

Zhang, MH, and JL Lin. 1997. “Constrained variational analysis of sounding data bases on column-integrated budgets of mass, heat, moisture, and momentum: Approach and application to ARM measurements.” *Journal of the Atmospheric Sciences* 54(11): 1503-1524, [doi:10.1175/1520-0469\(1997\)054<1503:CVAOSD>2.0.CO;2](https://doi.org/10.1175/1520-0469(1997)054<1503:CVAOSD>2.0.CO;2).

Zhang, MH, JL Lin, RT Cederwall, JJ Yio, and SC Xie. 2001. “Objective Analysis of ARM IOP Data: Method and Sensitivity.” *Monthly Weather Review* 129(2), 295-311, [doi:10.1175/1520-0493\(2001\)129](https://doi.org/10.1175/1520-0493(2001)129).

Zhu, P, CS Bretherton, M Kohler, A Cheng, A Chlond, Q Geng, P Austin, J-C Golaz, G Lenderink, A Lock, and B Stevens. 2005. “Intercomparison and interpretation of single-column model simulations of a nocturnal stratocumulus-topped marine boundary layer.” *Monthly Weather Review* 133(9): 2741-2758, [doi:10.1175/MWR2997.1](https://doi.org/10.1175/MWR2997.1).

Zuidema, P, H Xue, and G Feingold. 2008. “Shortwave radiative impacts from aerosol effects on shallow marine cumuli.” *Journal of the Atmospheric Sciences* 65(6): 1979-1990, [doi:10.1175/2007JAS2447.1](https://doi.org/10.1175/2007JAS2447.1).

Zuidema, P, Z Li, R Hill, L Bariteau, B Rilling, C Fairall, WA Brewer, B Albrecht, and J Hare. 2012. “On trade-wind cumulus cold pools.” *Journal of the Atmospheric Sciences* 69(1): 258-277, [doi:10.1175/jas-d-11-0143.1](https://doi.org/10.1175/jas-d-11-0143.1).



www.arm.gov

U.S. DEPARTMENT OF
ENERGY

Office of Science